https://ntrs.nasa.gov/search.jsp?R=19820006182 2020-03-21T10:08:44+00:00Z

NASA
TP
1958
c.1

NASA
Technical
Paper
1958

December 1981

TECH LIBRARY KAFB, NM
0134991

Comparison of Experimental and Theoretical Turbulence Reduction Characteristics for Screens, Honeycomb, and Honeycomb-Screen Combinations

James Scheiman

LOAN COPY: RETURN TO
AFWL TECHNICAL LIBRARY
KIRTLAND AFB, N. M.

NASA

TECH LIBRARY KAFB, NM

0134991

NASA
Technical
Paper
1958

1981

Comparison of Experimental and Theoretical Turbulence Reduction Characteristics for Screens, Honeycomb, and Honeycomb-Screen Combinations

James Scheiman
Langley Research Center
Hampton, Virginia

NASA
National Aeronautics
and Space Administration

Scientific and Technical
Information Branch

SUMMARY

A half-scale model of a portion of the NASA Langley 8-Foot Transonic Pressure Tunnel was used to conduct some turbulence reduction research using screens, honeycomb, and combinations thereof. The experimental results are compared with various theories. The axial turbulence reduction for screens agrees with the Prandtl theory, whereas the lateral turbulence reduction agrees with the Dryden and Schubauer theory. Screens alone reduce axial turbulence more than lateral turbulence. Honeycomb alone reduces lateral turbulence more than axial turbulence. Because of this difference, the physical mechanism for decreasing turbulence for screens and honeycomb must be completely different, and these mechanisms are speculated on herein. The turbulence reduction of a screen when placed downstream of the honeycomb is far better than that for the screen alone with the result that the honeycomb with a downstream screen is an excellent combination for reducing turbulence.

INTRODUCTION

A more energy efficient aircraft is becoming a desirable goal. One method of achieving this goal is to decrease the aircraft drag. It has been estimated that the overall aircraft drag can be reduced approximately 40 percent by achieving laminar flow over the relatively large wing area. (See ref. 1.) In order to be meaningful, laminar flow airfoil research tests must be conducted in a very low turbulence wind tunnel. One means of straightening the flow and decreasing wind-tunnel turbulence is to use screens and honeycomb as fluid flow manipulators, for example see references 2 and 3. Because of the pressure drop and additional power required to overcome the drag of the manipulators when they are installed in the flow stream, these manipulators are generally installed in the settling chamber area just upstream of the contraction in the lowest speed portion of the wind tunnel.

There are a number of theories available for predicting the performance, turbulence reduction and pressure loss, of various flow manipulators, for example, references 4 through 13. However, since many of the different theories are based on a given set of experimental results and are therefore empirical in nature, these different theories fail to predict consistently the turbulence reduction performance for a particular manipulator. For example, see references 5 through 10, and 13. Because of these inconsistencies, correlation of the data herein with the various theories was attempted and additional manipulator data were obtained. The results are reported herein.

The present tests were conducted with an available model flow duct used to evaluate turbulence reduction modifications for the Langley 8-Foot Transonic Pressure Tunnel. A discussion of the final manipulator configuration selected and a description of the flow duct used for the tests are presented in reference 14. Some testing experience directly related to the development of the final configuration is presented in reference 15.

The flow duct included a one-half scale simulated cooler and 45° turning vane. A porous plate with 45 percent open area was installed downstream of the 45° turning vane to serve as a uniform turbulence generator. Various combinations of honeycomb

and screen manipulators were tested. The mean test speed varied from 7.62 to 18.29 meters per second (25 to 60 feet per second). Both the axial turbulence and lateral turbulence were measured by using conventional hot wires. The turbulence reduction was averaged over the speed range, and the turbulence reduction results are correlated with various theories. Honeycomb alone, screens alone, and honeycomb-screen combinations were evaluated.

SYMBOLS

Values are given in both SI and U.S. Customary Units. The measurements and calculations were made in U.S. Customary Units.

B	measure of deflection of air defined by difference between upstream and downstream velocity normalized by upstream velocity, $0 < B < 1$ (see ref. 7)
D	screen wire diameter, cm (in.)
E	output voltage of hot wire, V
e	differential value of E, dE
e'	rms voltage perturbation, $\sqrt{\overline{e^2}}/E$
f	turbulence reduction factor, turbulence with manipulator divided by turbulence without manipulator
K	pressure-loss coefficient, $\Delta p/q$
K_o	constant value that K approaches at very high values of Reynolds numbers (see ref. 7)
L	integral length scale of initial turbulence, m (ft)
L_{kj}	hot-wire calibration constant, $k = 1$ denotes slope of equation (3); $k = 2$ denotes intercept of equation (3); $j = 2$ or 3 denotes one wire of cross-wire probe
ℓ	depth of honeycomb cell, m (in.)
M	screen mesh, wires/2.54 cm (wires/in.)
m	fluid mass-flow rate
n	number of data points
Δp	static-pressure loss across flow manipulator, N/m^2 (lb/ft^2)
q	dynamic pressure of fluid, $\frac{1}{2}\rho U^2$, N/m^2 (lb/ft^2)
R	Reynolds number

S_i, S_{ij} hot-wire calibration constants (see appendix), $i = 1$ denotes u'; $i = 2$ denotes v'; $j = 2$ or 3 denotes one wire of cross-wire probe

U mean fluid-flow velocity, m/s (ft/sec)

u axial velocity fluctuation

u' rms velocity perturbation in axial direction, $\sqrt{\overline{u^2}}/U^2$

v lateral velocity fluctuation

v' rms velocity perturbation in lateral direction, $\sqrt{\overline{v^2}}/U^2$

α ratio of flow angle of incidence with respect to normal to screen surface for upstream flow to angle of incidence for downstream flow

β screen porosity, screen projected open area divided by total area

δ angle of flow with respect to hot wire

ρ fluid mass density, kg/m^3 (lb/ft^3)

σ_x standard deviation of value of measured turbulence

$\sigma_{\bar{x}}$ standard deviation of mean value of measured turbulence

Subscripts:

m measured

nom nominal value

u axial turbulence

v lateral turbulence

t theoretical

Abbreviations:

HC honeycomb

rms root mean square

Designations:

4M, 8M, 20M, 28M, 36M, 42M screen-mesh designations (see table I)

1/16 HC, 1/8 HC, 1/4 HC, 3/8 HC honeycomb designations (see table I)

MODEL AND INSTRUMENTATION

The test facility consisted of a flow duct containing a half-scale model of the Langley 8-Foot Transonic Pressure Tunnel (TPT) cooling coils and 45° turning vanes. The cooling coils were simulated and were not used as heat exchangers. All tests were performed under adiabatic conditions. The duct cross section is 0.46 m (18.25 in.) square and thus only a small section of the full-scale tunnel is simulated. A sketch of the model is shown in figure 1. A porous plate 0.1588 cm (0.0625 in.) thick with 0.476-cm-diameter (0.188-in.) holes was installed. Alternate rows or columns of holes were staggered; the horizontal hole spacing was 0.711 cm (0.28 in.) and the vertical spacing was 1.123 cm (0.442 in.). The porous plate had a 45-percent open area and was installed 0.61 m (24 in.) downstream of the trailing edge of the 45° turning vane measured along the center line of the duct. This plate was installed to generate a turbulence above that of the basic duct and thereby to make the results more general rather than be specifically related to the 8-Foot TPT type cooler and turning vane.

The air drive system (sketched in fig. 1(a)) consisted of three tip-air-driven high-speed motors. The motor had a blade passage frequency between 2200 and 5867 Hz. The motors were enclosed in an acoustic-lined box with internal acoustic baffles to keep the motor noise from contaminating the measured turbulence data.

The dimensions of the screens chosen for evaluation are presented in table 1. The various mesh sizes were chosen to cover a wide range. A major consideration was the screen percent open area which must be kept subcritical (ref. 5), namely at least 58 percent open.

The screens were permanently mounted in square frames, with a frame thickness or screen spacing equal to between 80 and 100 screen mesh sizes. The data in reference 16 indicate that almost all the turbulence decay occurs within 50 to 75 screen mesh sizes downstream of the screen. Therefore, whenever multiple screens were being evaluated, the corresponding frame thickness provided assurance that turbulence was adequately decayed before the air flow encountered the next manipulator.

The honeycomb characteristics chosen for evaluation are also presented in table 1. The honeycomb material was aluminum or stainless steel. One primary criterion was that the ratio of honeycomb cell length to cell size be between 6 and 8 (based on information in ref. 16).

In general, the honeycomb was installed in the duct at the farthest upstream position of the manipulator section and the first following screen was positioned 0.3 m (1 ft) downstream of the downstream end of the honeycomb. (See fig. 1.) The turbulence decay data in reference 16 indicate almost complete decay at a distance of 23 to 25 cm (9 to 10 in.) downstream of a simulated honeycomb made of soda straws. This distance corresponds to about 50 soda-straw diameters or between 1 to 10 cell-depth dimensions. For the tests herein, the 0.3-m (1-ft) spacing corresponds to 32 to 200 cell diameters or 4.5 to 28 cell-depth dimensions, respectively, for the 3/8 to 1/16 cell size honeycomb. It is therefore assumed for the data presented herein for the honeycomb-screen combinations that the turbulence from the upstream honeycomb is almost completely decayed before encountering the first screen.

The instrumentation utilized in this experiment is indicated in figure 1(b). Two hot-wire probes were installed between the porous plate and the first manipulator. These hot-wire probes measured the axial turbulence and were used to verify that the turbulence upstream of the manipulators had a relatively constant value.

The remaining hot-wire probes were used to measure the axial and lateral turbulence downstream of the various manipulators. These hot wires were located 0.30 m (12 in.) downstream of the last downstream manipulator. All the hot wires had fixed locations during these tests and all the hot-wire anemometers were operated in the constant temperature mode. The downstream hot wires were isolated from wall vibrations by mounting them on a separate floor stand and using a soft rubber seal between the duct wall and hot-wire support arm. The tungsten wires were platinum coated and had a distance between supports of 1.5 mm (0.06 in.). The active wire sensing length was 1.25 mm (0.05 in.) and the wire diameter was 4 μm (0.00015 in.) resulting in a length-to-diameter ratio greater than 300. The single wires were aligned normal to their respective probe axes and the probe axes were aligned with the mean flow direction. The two cross wires were aligned in parallel planes with a spacing of 1 mm (0.04 in.). These planes and the axis of the probe were aligned with the mean flow direction. The hot-wire data were recorded with a high-pass 2-Hz and a low-pass 50-kHz filter. Typical spectra of the axial component of turbulence for various mean speeds upstream and downstream of a manipulator are shown in figures 2(a) and 2(b), respectively.

In addition to the hot-wire instrumentation, two standard acoustic microphones were used. Both microphones were mounted flush with the duct wall and were isolated from wall vibrations by using independent floor supports and a flexible rubber seal in the duct wall. One microphone was located approximately 0.41 m (1.33 ft) downstream of the center line through the trailing edge of the turning vane. The other microphone was located 0.53 m (1.75 ft) downstream of the most downstream hot wires. These microphones were used to detect acoustic noise within the duct which could affect the hot-wire (or turbulence) measurement. A more detailed discussion of this problem can be found in reference 15. A sketch of the general dimensions and instrumentation location is shown in figure 1(b). Typical spectra for the farthest downstream microphone for various speeds are shown in figure 2(c).

Three variable capacitance pressure transducers were used to measure static-pressure differences. One pressure transducer was used to determine the pressure difference across the manipulator. The other two were used to measure the static and difference between total and static pressures within the duct. Further details about the model or instrumentation can be found in reference 15.

HOT-WIRE MEASURING ACCURACY

To evaluate the accuracy of the hot-wire data, the data reduction equations were reviewed. (See appendix.) This review indicated that a direct evaluation of the sensitivity of the input parameters was not possible. Therefore, mean values of all the input variables were chosen. Then an arbitrary ±10-percent error in each variable was introduced, one variable at a time, into the data-reduction equations. The results are shown in figure 3. In figure 3(a), the resulting errors in axial and lateral turbulence for input error in the measured voltages are shown; in figure 3(b), the errors for input errors in the hot-wire calibration constants are shown. The results show the nominal (mean) value of turbulence and the ±10-percent error range. The figures show that the axial-turbulence (u') error generally stays within the ±10-percent band, whereas the lateral-turbulence (v') errors can be much larger than ±10 percent. The data reduction equations indicate that errors in measurement with the cross-wire probe will not affect the axial turbulence, but errors in the single-wire measurements will affect the lateral turbulence. In other words, it is more difficult to obtain accurate lateral turbulence than axial turbulence.

A further assessment of the accuracy was made as follows. Recall that two hot wires (single wire probes) were placed between the porous plate and the first manipulator. (These wires were used to verify that the turbulence leaving the porous plate and/or entering the manipulators was relatively constant.) The measured output from one (upstream) wire was tabulated over a 30-day period. This tabulation included 175 data points, 5 duct velocities, 2 different hot wires (one was broken during the time period), and many different manipulators. The repeatability of the data was evaluated statistically (i.e., the mean and standard deviation σ) for each of the five duct velocities. At a duct velocity of 18.3 m/s (60.0 ft/s), the scatter for 95 percent of the data (2σ) fell within ±12 percent of the mean; at 15.24 m/s (50.0 ft/s), ±5.7 percent; at 12.2 m/s (40.4 ft/s), ±4.5 percent; at 9.1 m/s (30.0 ft/s), ±4.7 percent; and at 7.62 m/s (25.0 ft/s), ±5.4 percent. Since the 18.3-m/s (60.0-ft/s) duct velocity was quite noisy and had a relatively large scatter, it was disregarded in most of the data presented herein. The standard deviation in the mean value of measured turbulence $\sigma_{\bar{x}}$ varies inversely as the square root of the number of data points averaged (i.e., $\sigma_{\bar{x}} = \sigma_x/\sqrt{n}$). In other words, the larger the number of values averaged the more accurate is the mean value (averaged number). By averaging the turbulence measurements for four velocities, 15.24, 12.2, 9.1, and 7.62 m/s (50.0, 40.0, 30.0, and 25.0 ft/s), the error in the mean value decreases by one-half. If the previously estimated errors for one hot wire are assumed to apply to each of the other wires in the system and the turbulence measurements for one manipulator are averaged over the four speeds, an estimated error of 2.5 to 3 percent results. Of course, averaging the measured turbulence levels for different mean duct velocities results in a pseudoturbulence level. However, this pseudoturbulence level will have less scatter (more accurate) and can be used for relative comparisons of different manipulator configurations.

During the test program, difficulties were sometimes encountered in overdriving the amplifiers for the hot-wire instrumentation. This difficulty was resolved by two techniques. The first was to use the dc offset available within the hot-wire signal-conditioning equipment. The second was to take two rms-output voltmeter readings: one reading was taken at the desired gain setting (determined by the tape recorder requirements) and the other at the next lower gain setting. These two output levels were compared (for acceptance), manually recorded, and averaged in the data-reduction process. In general, two additional data points were averaged at each duct speed. This averaging decreased the scatter (or error) in the reported turbulence further.

On the basis of the preceding discussion, it is concluded that the measured and average axial turbulence (pseudoturbulence) data presented have an uncertainty of approximately 2 percent. From the previous discussion of figure 3, it is estimated that the average lateral turbulence (pseudoturbulence) may have an error as high as 4 percent.

The hot wires will respond to acoustic waves as well as vorticity (turbulence). This problem can be minimized by keeping the acoustic energy well below the turbulent energy. In other words, with only a few turbulence manipulators (relative small turbulence reduction) and a small pressure drop (lower drive motor acoustic noise), the turbulence energy will be relatively high compared with the acoustic energy. A comparison of the microphone measurements downstream of the manipulator (fig. 2(c)) with the hot-wire-measured turbulence frequencies (figs. 2(a) and 2(b)) show that the acoustic energy has a relatively small effect on the overall hot-wire rms voltage output for the present tests.

TESTS

The tests were conducted by installing the manipulators, sealing the duct, and running the tests over the velocity range. At each duct velocity the output from the pressure transducers was read manually on digital voltmeters. The hot-wire rms voltage outputs were also recorded manually. The hot-wire and acoustic signals were then recorded on an FM tape recorder for later, more detailed, data analysis. For the porous plate only (no other flow manipulators), the measured axial and lateral turbulence at the farthest downstream station were equal (i.e., within the accuracy range) over the entire operating speed range. It was therefore assumed that turbulence was nearly isotropic entering the downstream flow manipulators.

DISCUSSION

Various turbulence reduction theories (refs. 5 through 10 and 13) have been compared with the experimental results obtained herein. The results presented are actually a small portion of the total amount of data accumulated during the test program. The results presented are typical of the data obtained. These results are presented in sections entitled: (1) "Review of Theories," (2) "Screens," (3) "Honeycomb and Honeycomb Screen Combinations," (4) "Spectra and Correlation," and (5) "General Comments."

Review of Theories

The most important parameter defining screen performance (turbulence reduction) is the pressure-loss coefficient K. The pressure-loss coefficient is defined as the static-pressure loss across the manipulator Δp divided by the dynamic pressure q of the mean flow through the manipulator. Some common assumptions in the theories are that the flow upstream of the manipulator is isotropic and homogeneous, that the turbulence level is small compared with the mean free-stream level, and that the fluid is incompressible.

In reference 8, the mean resistance of the screen to turbulence, or the energy change across the screen, KE_2' (where E_2' is at the station of the screen) is equated to the difference between the upstream turbulent energy E_1' and the downstream turbulent energy E_3' or $KE_2' = E_1' - E_3'$. It was reasoned in reference 8 that the turbulence downstream of the screen cannot change after it leaves the screen; in other words, change in turbulence due to the screens occurs on the upstream side only, i.e., $E_2' = E_3'$. Since the turbulence velocity is proportional to the square root of the turbulent energy, from the turbulent energy equation the turbulence reduction factor becomes $\frac{u_3'}{u_1'} = \frac{1}{\sqrt{1 + K}}$. The experimental data presented in references 5 and 8 seem to verify this theoretical reduction law.

In reference 4, Prandtl stated that screens can be used to obtain a more uniform velocity distribution across the duct section and that a moderate velocity difference is approximately lower by the factor $\frac{1}{1 + K}$. This factor has subsequently been shown to equal one of the boundaries for turbulence reduction across a screen. In reference 6, Collar used Bernoulli's equation to equate the loss in total head to the local pressure drop through the gauze (screen). He then used the momentum equation

to determine the increase in momentum of the fluid in accelerating through the reduced area of the gauze. Assuming that the perturbation velocities are small compared to the mean flow velocity, he showed that $\frac{v_3'}{v_1'} = \frac{2 - K}{2 + K}$

In reference 13, a more elaborate analysis was presented. Taylor and Batchelor accounted for the fact that if the flow is nonnormal to the manipulator upstream, it will be turned toward the normal downstream. Further, they showed from experimental data that for a given screen over a nominal velocity range, the ratio (α) of the flow-angle out of the screen (ϕ) to the flow angle into the screen (θ) is approximately constant. Further, from the test data (ref. 5) the ratio α equals $\frac{1.1}{\sqrt{1 + K}}$, and this ratio is approximately equal to the lateral turbulence reduction factor. By using potential flow theory and accounting for the boundary conditions on both sides of the screen, they showed (ref. 13) that the axial turbulence reduction factor squared was equal to

$$f_u^{\,2} = \frac{(1 + \alpha - \alpha K)^2 + 2\alpha^2}{(1 + \alpha + K)^2 - 4} + \frac{(1 + \alpha - \alpha K)^2 - 4\alpha^2}{(1 + \alpha + K)^2 - 4} \times$$

$$\frac{3}{2}(1 - \eta^2)\left[1 + \frac{\eta^2 - \xi^2}{2\eta} \ln \frac{\eta - 1}{\eta + 1}\right]$$

and the lateral turbulence reduction factor squared is equal to

$$f_v^{\,2} = \alpha^2 + \frac{1}{8}\left[(1 + \alpha - \alpha K)^2 - (1 + \alpha + K)^2 f_u^{\,2}\right]$$

where

$$\xi^2 = \frac{(1 + \alpha - \alpha K)^2}{(1 + \alpha - \alpha K)^2 - 4\alpha^2}$$

and

$$\eta^2 = \frac{(1 + \alpha + K)^2}{(1 + \alpha + K)^2 - 4}$$

As shown in reference 13, the results of these equations can be reduced to the axial turbulence reduction factor of

$$\frac{1 + \alpha - \alpha K}{1 + \alpha + K}$$

and the lateral turbulence reduction factor equal to α. By the definition of $\alpha = \frac{\phi}{\theta}$, α can vary between 0 and 1. In reference 13, Taylor and Batchelor show that when $\alpha = 0$, their axial turbulence reduction is identical with that of Prandtl (ref. 4), and when $\alpha = 1$, their reduction factor becomes identical to Collar (ref. 6). The theory in reference 13 is the only one that presents a lateral turbulence reduction factor.

Screens

Based on the turbulence reduction theories, the most important parameter for defining screen performance (turbulence reduction) is the pressure-loss coefficient K. In figure 4, the pressure-loss coefficient is plotted as a function of the duct velocity for various representative screens and screen combinations.

The flow pressure loss through a screen can be a function of numerous parameters, for example, screen solidity (ref. 13), Reynolds number (ref. 7), and Mach number (ref. 17). For the tests herein, the Reynolds number based on the screen wire diameter is relatively low, namely, from 100 to 600. Therefore, variations in the Reynolds number can have a large effect on the pressure loss, and the computed pressure-loss coefficient was determined by using the procedures in reference 7. In reference 7, the pressure-loss coefficient K is equal to

$$K = K_o + \frac{55.2}{R_w}$$

where

$$K_o = \left(\frac{1 - 0.95\beta}{0.95\beta}\right)^2$$

$$\beta = \frac{\text{Projected open area}}{\text{Total area}} = (1 - MD)^2$$

R_w = Reynolds number based on wire diameter

The variation of pressure loss across the screen with velocity is shown in figure 5, the corresponding calculated values (from ref. 7) are shown as dashed lines. The agreement with the measured results is not good, quantitative errors in the calculated results being as great as 50 percent, although the calculated results do show the correct trends with velocity and screen physical characteristics. The prediction from reference 7 is semiempirical as indicated by experimental verifying information. The lack of correlation with the data herein implies that the pressure drop across the screens may be dependent on other parameters not considered previously, such as upstream incoming turbulence level or scale of turbulence.

The measured turbulence reduction divided by the theoretical turbulence reduction is plotted in figure 6 as a function of test velocity. The theoretical turbulence reduction information was obtained from references 5 and 8, namely $\frac{1}{\sqrt{1 + K}}$. The results show both the axial u' and lateral v' turbulence reduction - u' and v' being the rms velocity perturbation along the respective axes. The measured turbulence reduction was obtained by measuring the turbulence with the manipulators installed and dividing these values by the measured turbulence without the manipulators. The measurements were made in the same physical location with or without the manipulators. If it is assumed that the upstream turbulence (upstream of the manipulators) is the same with and without the presence of the manipulators, then the previously described turbulence reduction is equal to the ratio of the downstream turbulence with the manipulator to the downstream turbulence without the manipulator; that is,

$$f_u = \frac{\left(\frac{u' \text{ upstream}}{u' \text{ downstream}}\right)_{\text{without manipulator}}}{\left(\frac{u' \text{ upstream}}{u' \text{ downstream}}\right)_{\text{with manipulator}}}$$

$$f_u = \frac{u' \text{ downstream with manipulator}}{u' \text{ downstream without manipulator}}$$

Recall that one of the upstream hot wires was used to verify that the turbulence was constant for all manipulators, including an open duct; therefore, this assumption has been verified at least for the axial component. Perfect correlation would result in a value of one for the ordinate in figure 6. The important point in figure 6 is that the lateral turbulence reduction v' is predicted fairly well by the theory, whereas the measured axial turbulence reduction is approximately 25 percent lower than the values predicted by theory. The axial and lateral turbulence do not have the same reduction. If the measured and the theoretical reduction varied with the same function of speed, then the ratio of these two reduction factors would be independent of speed. Even though there is considerable scatter in the data in figure 6, the mean data do not vary much with speed.

Shown in figure 7 is a plot of the turbulence reduction factor for various screen mesh sizes. Values of both axial and lateral turbulence reduction are shown. As discussed with regard to figure 6, the ratio of measured and theoretical turbulence reduction does not vary significantly with speed; in order to minimize the experimental scatter, improve the accuracy, and simplify the evaluation of the correlation as a function of screen mesh size, the data were averaged over the speed

range. The theoretical turbulence reduction factors presented are also based on the arithmetic average value of the pressure-loss coefficient over the speed range. Figure 7 is presented to compare, more easily, the different theoretical predictions for different screens. The theory from references 5 and 8, namely $\frac{1}{\sqrt{1 + K}}$, is again plotted with the same conclusion as in figure 6. Because of the lack of correlation for the axial turbulence, the theory in reference 4, namely $\frac{1}{1 + K}$, is also shown. This reference presents the reduction as a smoothing effect of the mean flow and not as a turbulence reduction factor. However, reference 13 implied that the factor could be used as a turbulence reduction factor (this is discussed in more detail later in this report). This reduction factor only applies to axial turbulence. A comparison of this theory (in ref. 4) with the measured results in figure 7 shows improved correlation with the measured axial turbulence reduction data.

Also shown in figure 7 is the theoretical turbulence reduction using the theory from reference 6, namely a reduction factor equal to $\frac{2 - K}{2 + K}$. This theory and that presented in reference 4 are shown in reference 13 to be degenerate cases of the more general theory, namely $\frac{1 + \alpha - \alpha K}{1 + \alpha + K}$. In reference 13, α is experimentally determined to be equal to $\frac{1.1}{\sqrt{1 + K}}$. These theoretical results are also shown in figure 7.

The theory in reference 7 is derived on the basis of smoothing of axial flow nonuniformities rather than turbulence reduction (Case (i) in ref. 7.) The final results are

$$\frac{u'_{downstream}}{u'_{upstream}} = \frac{2 - B - K(1 - B)}{2 - B + K}$$

where

$$0 < B < 1$$

For $B = 0$ the theory degenerates to the theory in reference 6 and for $B = 1$ the results are identical to the theory in reference 4. This theory is not shown in figure 7 because the two extremes are already shown. Figure 7 shows that the measured axial turbulence reduction seems to agree with the theory of reference 4 and the measured lateral turbulence reduction seems to agree with the theory of reference 5.

In reducing turbulence, multiple screens are often used (ref. 5). From the previous discussion, it is seen that the axial and lateral turbulences are not reduced the same amount after the flow has passed through one screen. (See fig. 7.) However, almost all the turbulence reduction theories assume that the upstream turbulence is isotropic. After the fluid passes through one screen, this flow requires sufficient distance to become isotropic for the succeeding screens. With

this precaution, the correlation with available theories will proceed by assuming that the upstream turbulence for each succeeding screen is isotropic.

A correlation of the measured and theoretical turbulence reduction factor averaged over the speed range for multiple screens is presented in figures 8 and 9. The theories from references 4 and 5 are presented because they agreed with measured turbulence reduction in the axial and lateral directions, respectively (fig. 7). The order of the first four screen configurations on the abscissa of figure 8 was selected to indicate the effect of adding screens in series. In figure 8 all screens had a 10.2-cm (4-in.) separation distance, except the one case that will be discussed subsequently. When using multiple screens, it is possible to estimate the theoretical performance by two methods. First, the recommended procedure (ref. 8) is to assume that each screen acts independently and compute the reduction factor of each screen separately, and then multiply these reduction factors together $\left(\text{i.e., } \prod \frac{1}{\sqrt{1 + K_i}}\right)$. The second possibility is to assume that the total pressure-loss coefficient is equal to the sum of those of the individual screens and proceed to compute the reduction factor for the equivalent system $\left(\text{i.e., replace the individual screens with one screen that has a pressure loss equal to the sum of the individual screens, } \frac{1}{1 + \Sigma K}\right)$. Both of these estimates are presented in figure 8. As expected, the correlation indicates that the first procedure results in the best correlation, namely to assume that each screen operates as an independent unit. Also, it appears that the axial and lateral turbulence reduction agrees best with the theories in references 4 and 5, respectively. Further, as the number of screens increases, the theory in reference 4 is somewhat optimistic and reference 5 is less optimistic as compared with the experimental data. The last two screen test conditions, shown in figure 8, are for the two screens with a 20.3 cm (8 in.) spacing and for the two screens the same distance apart but one screen mesh rotated 45° with respect to the other. The test data show that there is very little difference in turbulence reduction for either of these last two conditions compared with that for the two screens with a 10.2 cm (4 in.) spacing.

Additional data using multiple screens with a much coarser mesh are presented in figure 9. The resulting correlation again indicates that the lateral turbulence reduction agrees well with the theory in reference 5. Also, the axial turbulence reduction seems to agree best with the theory of reference 4, however, the correlation is not as good as with the lateral turbulence.

Honeycomb

There are only limited data available about the performance of honeycomb in the literature. Figure 10 is a plot of the static-pressure drop as a function of velocity for the various cell-diameter and cell-depth honeycombs used in the study. The data were obtained from an interpolation and extrapolation of the manufacturer's results. The only data measured herein were for the 1/4 HC (1/4-in. honeycomb). All the honeycomb depths tested were chosen with a ratio of cell length to cell diameter between 6 and 8. Presented in reference 10 is a theory for determining the pressure loss for a honeycomb that has fully developed turbulent flow within each cell but these data are not included in figure 10. This is because the cell-length Reynolds number for the tested 1/4 HC is about 40 000, and from reference 10 the cell flow would not be fully turbulent; therefore, this theory is not expected to apply. The

comparison of the manufacturer's data with the measured honeycomb pressure loss shown in figure 10 is not very good.

Another method for estimating the pressure loss for the honeycomb is suggested and described as follows. This method is valid for Reynolds numbers (R), based on the cell depth, values less than about 100 000. Then it can be assumed that the cell flow is two dimensional with a laminar boundary layer. The equivalent skin friction based on wetted area is determined from $1.328/R^{1/2}$ (e.g., see ref. 18). In turn, the total wetted honeycomb surface area for one unit of cross sectional area and the drag or pressure loss per unit of area is determined. The results of applying this procedure to the 1/4 HC are shown in figure 10. The agreement is good.

When honeycomb is used to reduce turbulence, it is usually used in combination with screens. Figure 11 presents the measured turbulence reduction for honeycomb alone and for honeycomb with various downstream screen combinations. In addition, various theoretical reduction factors are presented.

As mentioned previously, there is very little experimental or theoretical honeycomb turbulence reduction information available. Since there is no theoretical design information available (except ref. 10), it might be constructive to use the theory for screens to predict the performance of honeycomb and honeycomb screen combinations. A review of the theoretical derivations for the turbulence reduction for screens indicates that the details of the manipulator are very general, that is, a device with a pressure drop. In fact, in reference 13, the turbulence reduction is developed as a function of a parameter α. As by definition, α is equal to the ratio of the flow angle of incidence with respect to the normal existing in the manipulator to the flow angle of incidence with respect to the normal entering the manipulator. For honeycomb, if the flow always exits normal and therefore $\alpha = 0$, then the theoretical turbulence reduction is identical to that in reference 4, namely $\frac{1}{1 + K}$. Also, if there is no turning of the flow in going through the manipulator, the turbulence reduction is identical to that in reference 6, namely $\frac{2 - K}{2 + K}$. Both of these limits are presented in figure 11. Also, since screens are involved, the theory in reference 5 is shown (recall that this theory predicts the lateral turbulence reduction for screens adequately). The decay requirements described in reference 16 have been satisfied as discussed in the section entitled "Model and Instrumentation." The theoretical and experimental turbulence reduction in figure 11 show poor correlation. In particular, the measured axial and lateral turbulence both are lower than the theory for honeycomb alone and for honeycomb with screens. Note that the turbulence downstream of the honeycomb alone is not isotropic since the axial and lateral turbulence are not equal. This turbulence is also the upstream turbulence for the screens in the honeycomb-screen combinations. Because of the lack of correlation with the honeycomb alone, the data were retabulated and plotted in figure 12.

The data of figure 12 are presented with the turbulence shed from the honeycomb representing the duct turbulence without the manipulator, and the turbulence downstream of the honeycomb and screen combination representing the turbulence with the manipulator. In other words the turbulence downstream of the honeycomb replaced the "baseline" turbulence of the empty duct. The correlation of theory and experiment in figure 12 is not good. The theory in reference 6 is optimistic for the 28M and 36M screens. One very important point in figures 11 and 12 is that, with honeycomb alone or with the honeycomb-screen combination, the measured lateral

turbulence is reduced more than the axial turbulence. This effect is unlike screens alone where the axial turbulence is reduced more than the lateral turbulence. This fact implies that the mechanism by which these two manipulators (honeycomb and screens) reduce turbulence are different.

Figures 13 and 14 present plots of the turbulence reduction ratio for various honeycomb cell sizes. The results are for a combination of honeycomb and screens. The data in figure 13 were obtained with a 2-Hz high-pass filter and in figure 14 with a 100-Hz filter. These data were obtained to determine if there is an optimum honeycomb cell size for the same input turbulence. Recall that all the data presented have a ratio of honeycomb cell length to cell diameter between 6 and 8. It appears that the 1/8 HC and screen combination may provide the best performance; however, the differences are not great enough to reach any conclusion. It is possible that the incoming turbulence scale has an effect on honeycomb cell size and subsequent performances to reduce the v' component.

Spectra and Correlations

This section presents representative spectra amplitude as a function of frequency for the hot-wire data. All the plots presented are log-log plots and all spectra are for a duct speed of 18.2 m/s (60 ft/s). The spectra are presented to aid in determining the mechanism and to reinforce the previously described findings concerning screens and honeycomb turbulence reduction. The u' spectra were obtained from an analysis of the recorded single hot-wire output. The v' spectra were obtained from an analysis of the recorded difference between the two cross hot-wire signals. The latter procedure requires that the two cross wires have the same sensitivity, which they do not. However, the data used to represent the resulting lateral turbulence spectra presented do provide general trend information. Since the levels presented do not include the hot-wire sensitivities, the ordinate scale of the spectra is relative rather than absolute.

The axial and lateral spectra for screens alone are shown in figures 15(a) and (b), respectively. The screen data can be compared with the data for the open duct (porous plate) which are shown as a solid line in the figures. The 42M screen (42 wires per inch (2.54 cm)) reduces the u' component of turbulence more than the 8M screen. (See fig. 15(a).) This is as expected because the pressure-loss coefficient for the 42M screen is larger than that for the 8M screen. Screens alone reduce the level of turbulence at frequencies below 1000 Hz. The axial turbulence is reduced more than the lateral turbulence, as was shown previously for the averaged rms turbulence.

Spectra for the 1/4 HC axial and lateral turbulence are presented in figures 16(a) and (b), respectively. Two different curves for the honeycomb are shown with the hot wire 0.30 m (12 in.) and 0.91 m (36 in.) downstream of the honeycomb. As shown previously, the honeycomb alone decreases the lateral turbulence more than the axial turbulence. Further, as might be expected, figure 16(b) shows that the honeycomb reduced the large-scale low frequencies much more than the small-scale high-frequencies of turbulence. In fact, some of the small-scale high-frequency lateral turbulence (scale smaller than the honeycomb cell size) could pass right through the honeycomb. The small-scale high-frequency turbulence is the turbulence that decays most rapidly due to fluid viscosity. Comparing the curves for the 0.30-m (12-in.) and the 0.91-m (36-in.) distance downstream of the honeycomb in figure 16 shows that the high-frequency turbulence decays the most rapidly. At the 0.30-m (12-in.) distance, the honeycomb actually increases the turbulence level for the

v' component above that of the open duct for frequencies above about 2000 Hz. This implies that the honeycomb transfers the large-scale v' turbulent energy to the small-scale high frequency region. (Generally it is the large-scale eddies that contain most of the turbulent energy.) Comparing figures 15 and 16, it is evident that, because of the difference in the spectra downstream of the two types of manipulators, the turbulence reduction mechanism for screens and honeycomb is different.

This same effect can be seen more clearly in figure 17 where the spectra for the screen alone and honeycomb alone for the 0.30-m (12-in.) distance are replotted on the same figure. As indicated previously, the screen reduces the turbulence level rather uniformly across the spectra. Whereas the honeycomb alone reduces the turbulence level mostly in the low-frequency portion of the spectra. It is the low-frequency portion of the spectra where the energy-containing eddies exit.

Spectra for the axial and lateral turbulence for honeycomb alone and honeycomb and screen combinations are presented in figure 18. Recall that the hot wire is always 0.30 m (12 in.) downstream of the last manipulator; therefore, for the honeycomb screen combinations the hot wire is farther downstream of the honeycomb alone. Thus, the small-scale high-frequency turbulence downstream of the honeycomb has had more time to decay. (See fig. 16.) Figure 18 shows that the previously described separate honeycomb and screen mechanisms for reducing turbulence are present.

Note that the spectra show the existence of a discrete frequency at about 450 Hz that becomes more pronounced as the overall level of turbulence is reduced. This frequency is due to a standing acoustic wave within the duct and is described more fully in reference 15.

Information about the integral length scale of turbulence is provided by figures 19 and 20. The integral time scale is usually defined as the area under the autocorrelation curve. For the case herein, the single hot wire which measured the u' component of turbulence was used to determine the autocorrelation curve, with the integral length scale being determined by multiplying the integral time scale by the velocity.

Shown in figure 19 is a plot of the integral length scale against the duct velocity. The integral scale for the open duct and numerous combinations of screens only are presented. A least-squares-fit straight line is drawn through the open-duct data and all the screen data. The integral length scale can be directly related to the turbulence spectra. For example, a relatively small integral scale is associated with high-frequency turbulence, whereas a large integral scale is associated with low-frequency turbulence.

A great deal of scatter in the data is shown in figure 19 although the least-squares-fit straight line indicates that screens seem to decrease the scale of turbulence when comparing screens and open-duct data. This implies that the overall effect of adding screens is to decrease the low frequencies more than the high frequencies. The intermediate effect of adding screens may be to decrease the lower frequencies of turbulence and to reintroduce small-scale turbulence from the wires. The previously described spectra of turbulence indicated that for screens the overall rms levels were decreased and the integral scale indicates that the overall frequency content is shifted to the higher frequencies.

Since the hot wire was at a constant distance downsteam of the last screen, the variation of integral length scale of turbulence with speed must be interpreted carefully because the time required for the fluid to traverse the constant distance to the hot wire decreases as the speed increases. Thus, as speed increases, there is less time for viscous decay, and it is the higher frequencies that decay more rapidly due to viscous decay.

Shown in figure 20 is a plot of the integral length scale of turbulence as a function of velocity, for honeycomb only and various honeycomb-screen combinations. A least-squares-fit straight line is drawn through the open-duct and the honeycomb data at the two downstream distances. The large increase in the integral length scale for the honeycomb at the two distances downstream is an indication of the rapid viscous decay of the high frequencies of turbulence. The relatively large difference in integral length scale of turbulence between the 0.30 m (12 in.) and 0.91 m (36 in.) indicates that the high-frequency turbulence decayed while the fluid traversed the extra distance.

General Comments

The previously presented turbulence reduction has been replotted in figures 21 and 22 in order to obtain a different perspective. The different theories in figure 21 show a large variation in predicted turbulence reduction. More disturbing is the existence of experimental data, presented in many of the referenced reports that support the validity of each individual theory. For example, references 5 and 8 present data that correlate with the theory in reference 13. Further, references 6, 7, 8, 9, and 13 present data to correlate with the respective theories presented. In most cases, the theories presented are quite simple potential flow solutions assuming an inviscid fluid. The Reynolds number effect, which is a viscous effect, discussed previously with regard to the screen pressure loss has been neglected in the theories. The pressure-loss coefficient which is obviously an important parameter for smoothing out the mean stream flow may not be the primary parameter for decreasing turbulence. Certainly, scale of turbulence, in general, is expected to be much smaller than the general scale of mean flow nonuniformities. Using only the rms value of turbulence in only the axial direction does not provide a very thorough definition of the complete three-dimensional vorticity field. Apparently the theories greatly simplify a very complex problem and provide a large variation in the predicted turbulence reduction.

Figure 22 is a plot of the turbulence reduction factor for honeycomb as a function of the pressure-loss coefficient. One of the theoretical curves is from reference 4 or reference 13 with $\alpha = 0$. The other theoretical curves were obtained from reference 10. The theory in reference 10 is a function of the pressure-loss coefficient and ratio of the internal length scale of turbulence to cell length L/ℓ. For the tests conducted herein, this ratio is estimated to be 0.4 and 0.7; therefore, the theoretical curves for these ratios are presented.

Reference 10 assumes that the cell flow is fully turbulent and shows that the honeycomb completely suppresses the transverse component of the velocity immediately downstream of the honeycomb. The data presented herein were measured 30.0 cm (12 in.) downstream of the honeycomb; therefore, if the lateral turbulence was completely suppressed immediately downstream of the honeycomb, the fluid would still have some time to become isotropic by the time it reached the measuring station. The test data herein certainly show that the honeycomb decreases the lateral turbulence more than the axial turbulence. (See fig. 11.)

The one test point, for the honeycomb alone, in figure 22 does not correlate with the theories presented. The theory in reference 4 is pessimistic and the theory in reference 10 is very optimistic. The flow within the honeycomb cell for the data presented was not fully turbulent and therefore the prediction in reference 10 is not expected to apply. There is no theory available for predicting the turbulence reduction of the honeycomb when the cell flow is laminar.

The data in figure 11 for honeycomb alone indicate that the honeycomb alone outperforms all the screen theories. Previously, it was shown that for screens alone, the axial turbulence decreases as $\frac{1}{1 + K}$ and the lateral turbulence decreases as $\frac{1}{\sqrt{1 + K}}$. Figure 12 shows that screens behind the honeycomb perform as $\frac{2 - K}{2 + K}$, which is better than screens alone. This implies that the turbulence reduction for screens is a function of the upstream turbulence in addition to the pressure-loss coefficient. None of the available theories include the upstream turbulence parameter as a variable.

Figures 6 through 9 show that screens alone reduce the axial turbulence more than the lateral turbulence. Figure 11 shows that for honeycomb alone, the lateral turbulence is reduced more than the axial turbulence. (Ultimately, the turbulence is converted into heat by means of fluid viscosity.) Both types of manipulators reduce turbulence by changing the form of the turbulence and encouraging viscous action. For the same pressure-loss coefficient, it appears, based on the present data, that the best turbulence reduction can be obtained with a honeycomb and downstream screen combination.

Because of the difference in turbulence reduction factors for screens alone, honeycomb alone, and screens in combination with honeycomb, their mechanism of reducing turbulence must be different. In fact, the mechanism for manipulating the turbulence is quite complex and little understood. Because of the laws of energy and momentum conservation, the manipulators basically change the characteristics of the turbulence. In addition, the manipulators create their own shed turbulence which is added to the flow stream. During this flow manipulation, viscosity is acting continuously but not equally on all frequencies and/or scales of the turbulence.

Assuming for the moment that the turbulence is very low frequency, then the behavior of the manipulator due to mean velocities only can be used to describe the behavior due to turbulence. Because of the honeycomb cell depth, it becomes difficult to imagine how any mean lateral velocity can exit downstream of the honeycomb. On the other hand, it is difficult to imagine how the honeycomb can modify the axial velocity distribution since the pressure loss is quite small but not negligible. Screens operating with an axial velocity variation will have a tendency to smooth out (spread out) the higher velocity regions into the lower velocity regions and result in a more uniform flow. This difference in performance of screens and honeycomb arises because of the relatively higher pressure loss across the screens as compared with that across the honeycomb. As the mean flow angle with respect to the normal to the screen increases, the openness area of the screen decreases as the cosine of the angle with respect to the normal. Therefore, screens will not be expected to turn or straighten the flow dramatically as compared with honeycomb. The behavior of the mean flow is now used to describe the behavior of turbulent velocities. This information will then be applied to the manipulator performance described herein.

The test data indicate that for screen alone, the axial turbulence is reduced more than the lateral turbulence. This information is consistent with the expected behavior of screens based on these deductions of mean flow. Further, from the test data, it appears that the honeycomb is an excellent suppressor of lateral turbulence; this is also consistent with the deductions of mean flow. However, the experimental data indicate the honeycomb alone is a good suppressor of axial turbulence which is inconsistent with the mean flow deduction. However, by including viscous effects, this behavior could be visualized as greatly reducing lateral turbulence directly with a subsequent reduction in axial turbulence as a result of an exchange of energy between axes as the turbulence tends to become isotropic downstream. Such a mechanism might explain the fact brought out in connection with figure 11 that honeycomb reduced axial turbulence as much as a screen while reducing lateral turbulence even more. Therefore, screens and honeycomb behave differently. Screens are more effective in reducing axial turbulence and the honeycomb is more effective in reducing lateral turbulence.

The data show that screens downstream of the honeycomb have a better performance than screens alone. It appears that turbulence downstream of the honeycomb is higher in the axial direction than in the lateral direction, and it is axial turbulence that screens are most capable of reducing. Therefore, the combination of honeycomb to reduce the lateral turbulence followed by a screen to reduce the axial turbulence left by the honeycomb provides an excellent combination for reducing overall turbulence.

CONCLUDING REMARKS

Tests of screens, honeycomb, and various combinations of these turbulence manipulators have been conducted. The axial and lateral turbulence and pressure loss for these manipulators have been measured. Various theories intended to predict the turbulence reduction are discussed and compared with experimental results. For the same isotropic upstream turbulence, screens reduce axial turbulence more than lateral turbulence. The axial turbulence reduction for screens agrees with the Prandtl theory $\frac{1}{1 + K}$, whereas the lateral turbulence reduction agrees with the Dryden and Schubauer theory $\frac{1}{\sqrt{1 + K}}$ (where K is the pressure-loss coefficient). Honeycomb, on the other hand, reduces the lateral turbulence more than the axial turbulence. Because of this difference, the physical mechanism for decreasing turbulence for screens and honeycomb must be completely different, and these mechanisms are speculated on herein. The turbulence reduction of a screen when placed downstream of a honeycomb is far better than that for the screen alone with the result that the honeycomb with a downstream screen is an excellent combination for reducing turbulence.

Langley Research Center
National Aeronautics and Space Administration
Hampton, VA 23665
November 20, 1981

APPENDIX

EQUATIONS FOR AXIAL AND LATERAL TURBULENCE MEASUREMENT

The equations derived in this appendix were used to determine the axial and lateral turbulence from a single wire at 90° to the flow and to cross wires at some angle to the flow. The equations are standard equations (for example, see ref. 19) for using hot wires in a constant temperature mode and are presented herein for completeness. The output voltage is

$$E = f(m,\delta)$$

where

m fluid mass-flow rate, ρU

δ angle of flow with respect to hot wire

The differential of E can be written as

$$dE = \frac{\partial E}{\partial m} dm + \frac{\partial E}{\partial \delta} d\delta$$

For the low airspeeds used herein ($U < 30.0$ m/s (100.0 ft/s), it is permissible to assume that the density is constant so that

$$dE = \frac{\partial E}{\partial U} dU + \frac{\partial E}{\partial \delta} d\delta$$

and hence

$$\frac{dE}{E} = \frac{(1/E)\ \partial E}{(1/U)\ \partial U} \frac{dU}{U} + \frac{(1/E)\ \partial E}{\partial \delta} d\delta$$

Let $e = dE$ and $u = dU$ so that

$$\frac{e}{E} = \frac{\partial \ln E}{\partial \ln U} \frac{u}{U} + \frac{\partial \ln E}{\partial \delta} d\delta$$

APPENDIX

Assume that u and v are small perturbations about the mean

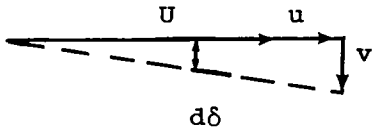

If the flow angle is $d\theta = \text{arc tan } \frac{v}{U + u} \approx \frac{v}{U}$, then

$$\frac{e}{E} = \frac{\partial \ln E}{\partial \ln U} \frac{u}{U} + \frac{\partial \ln E}{\partial \delta} \frac{v}{U}$$

Let $e' = \frac{\sqrt{e^2}}{E}$, $u' = \frac{\sqrt{u^2}}{U}$, and $v' = \frac{\sqrt{v^2}}{U}$, where $\sqrt{e^2}$, $\sqrt{u^2}$, and $\sqrt{v^2}$ represent the rms values and multiply by 100 so that e', u', and v' represent percent rms turbulence:

$$e' = \frac{\partial \ln E}{\partial \ln U} u' + \frac{\partial \ln E}{\partial \delta} v'$$

Define the hot-wire sensitivities by S_1 and S_2, where

$$S_1 = \frac{\partial \ln E}{\partial \ln U} \qquad \text{(Sensitivity of wire to } U\text{)}$$

$$S_2 = \frac{\partial \ln E}{\partial \delta} \qquad \text{(Sensitivity of wire to } \delta\text{)}$$

These sensitivities will be determined by calibration of each individual hot wire. The data reduction equation then becomes

$$e' = S_1 u' + S_2 v'$$

Assume a three-wire system where the axis of one wire is at 90° to the flow and the other two wires are at about ±45° to the flow. The first wire will not respond to v ($S_2 \approx 0$); therefore,

$$e_1' = S_1 u'$$

APPENDIX

For wires 2 and 3:

$$e_2' = S_{12}u' + S_{22}v'$$

$$e_3' = S_{13}u' + S_{23}v'$$

Solve the single-wire equation for the u' component of turbulence

$$u' = \frac{e_1'}{S_1} \tag{1}$$

Square the two equations for the cross wires, multiply the first by $S_{13}S_{23}$ and the second by $S_{12}S_{22}$, and subtract the two equations so that the cross-product term is eliminated and

$$S_{13}S_{23}\left(e_2'^2 - S_{12}^2u'^2\right) - S_{12}S_{22}\left(e_3'^2 - S_{13}^2u'^2\right) = \left(S_{13}S_{23}S_{22}^2 - S_{12}S_{22}S_{23}^2\right)v'^2$$

Solve for v' and recall that the u' component of turbulence is known from the single wire (eq. (1)) so that

$$v'^2 = \frac{S_{13}S_{23}\left(e_2'^2 - S_{12}^2u'^2\right) - S_{12}S_{22}\left(e_3'^2 - S_{13}^2u'^2\right)}{\left(S_{13}S_{23}S_{22}^2 - S_{12}S_{22}S_{23}^2\right)} \tag{2}$$

This is the lateral component of turbulence.

The sensitivity of the single wire S_1 is determined by measuring the wire output (dc volts) over the velocity range U of interest, and determining the slope for a plot of $\ln E$ against $\ln U$ $\left(S_1 = \frac{\partial \ln E}{\partial \ln U}\right)$. Similarly, the sensitivities to U, S_{12} and S_{13}, are determined for the other two cross wires. The sensitivities S_{22} and S_{23} are determined by measuring the cross-wire dc-voltage output for a number of small angle variations δ. These sentivities are then determined from the slope of a plot of $\ln E$ against δ $\left(S_2 = \frac{\partial \ln E}{\partial \delta}\right)$ for the two cross wires. All these sensitivities must be measured in a relatively low-turbulence environment. Since these sensitivities (S_{22} and S_{23}) vary somewhat with speed, they are determined for various speeds and they are expanded and redefined as follows:

$$\left.\begin{aligned} S_{22} &= L_{12}U + L_{22} \\ S_{23} &= L_{13}U + L_{23} \end{aligned}\right\} \tag{3}$$

REFERENCES

1. Braslow, Albert L.; and Muraca, Ralph J.: A Perspective of Laminar-Flow Control. AIAA Paper 78-1528, Aug. 1978.

2. Young, A. D.; and Maas, J. N.: The Behaviour of a Pitot Tube in a Transverse Total-Pressure Gradient. R. & M. No. 1770, British A.R.C., 1937.

3. Hall, A. A.: Measurements of the Intensity and Scale of Turbulence. R. & M. No. 1842, British A.R.C., 1938.

4. Prandtl, L.: Attaining a Steady Air Stream in Wind Tunnels. NACA TM 726, 1933.

5. Schubauer, G. B.; Spangenberg, W. G.; and Klebanoff, P. S.: Aerodynamic Characteristics of Damping Screens. NACA TN 2001, 1950.

6. Collar, A. R.: The Effect of a Gauze on the Velocity Distribution in a Uniform Duct. R. & M. No. 1867, British A.R.C., 1939.

7. Davis, G. De Vahl: The Flow of Air Through Wire Screens. Hydraulics and Fluid Mechanics, Richard Silvester, ed., Macmillan Co., 1964, pp. 191-212.

8. Dryden, Hugh L.; and Schubauer, G. B.: The Use of Damping Screens for the Reduction of Wind-Tunnel Turbulence. J. Aeronaut. Sci., vol. 14, no. 4, Apr. 1947, pp. 221-228.

9. Batchelor, G. K.: The Theory of Homogeneous Turbulence. Cambridge Univ. Press, 1953.

10. Lumley, J. L.; and McMahon, J. F.: Reducing Water Tunnel Turbulence by Means of a Honeycomb. Trans. ASME, Ser. D: J. Basic Eng., vol. 89, Dec. 1967, pp. 764-770.

11. Bradshaw, P.: The Effect of Wind-Tunnel Screens on Nominally Two-Dimensional Boundary Layers. J. Fluid Mech., vol. 22, pt. 4, Aug. 1965, pp. 679-687.

12. Kistler, A. L.; and Vrebalovich, T.: Grid Turbulence at Large Reynolds Numbers. J. Fluid Mech., vol. 26, pt. 1, Sept. 1966, pp. 37-47.

13. Taylor, G. I.; and Batchelor, G. K.: The Effect of Wire Gauze on Small Disturbances in a Uniform Stream. Q. J. Mech. & Appl. Math., vol. 2, pt. 1, Mar. 1949, pp. 1-29.

14. McKinney, Marion O.; and Scheiman, James: Evaluation of Turbulence Reduction Devices for the Langley 8-Foot Transonic Pressure Tunnel. NASA TM-81792, 1981.

15. Scheiman, James: Considerations for the Installation of Honeycomb and Screens To Reduce Wind-Tunnel Turbulence. NASA TM-81868, 1981.

16. Loehrke, R. I.; and Nagib, H. M.: Experiments on Management of Free-Stream Turbulence. AGARD R-598, Sept. 1972.

17. Pinker, R. A.; and Herbert, M. V.: The Pressure Loss Associated With Compressible Flow Through Square-Mesh Wire Gauzes. N.G.T.E. R.281, British Min. Aviat., June 1966.

18. Schlichting, Hermann (J. Kestin, transl.): Boundary-Layer Theory, Sixth ed. McGraw-Hill Book Co., Inc., c.1968, p. 128.

19. Hinze, J. O.: Turbulence. McGraw-Hill Book Co., Inc., 1959.

TABLE 1.- PHYSICAL PROPERTIES OF FLOW MANIPULATORS

(a) Screens

Designation	Mesh, wires/in. (2.54 cm)	Wire diameter		Open area, percent
		cm	in.	
4M	4	0.1270	0.0500	64
8M	8	.0660	.0260	63
20M	20	.0230	.0090	67
28M	28	.0190	.0075	62
36M	36	.0165	.0065	59
42M	42	.0140	.0055	59

(b) Honeycomb

Designation	Cell size		Cell length		Material gage		Cell length / Cell size
	cm	in.	cm	in.	mm	in.	
1/16 HC	0.159	1/16	1.27	0.50	0.0254	0.001	8
1/8 HC	.318	1/8	1.90	.75	.0254	.001	6
1/4 HC	.635	1/4	3.81	1.50	.0762	.003	6
3/8 HC	.952	3/8	7.62	3.00	.0762	.003	8

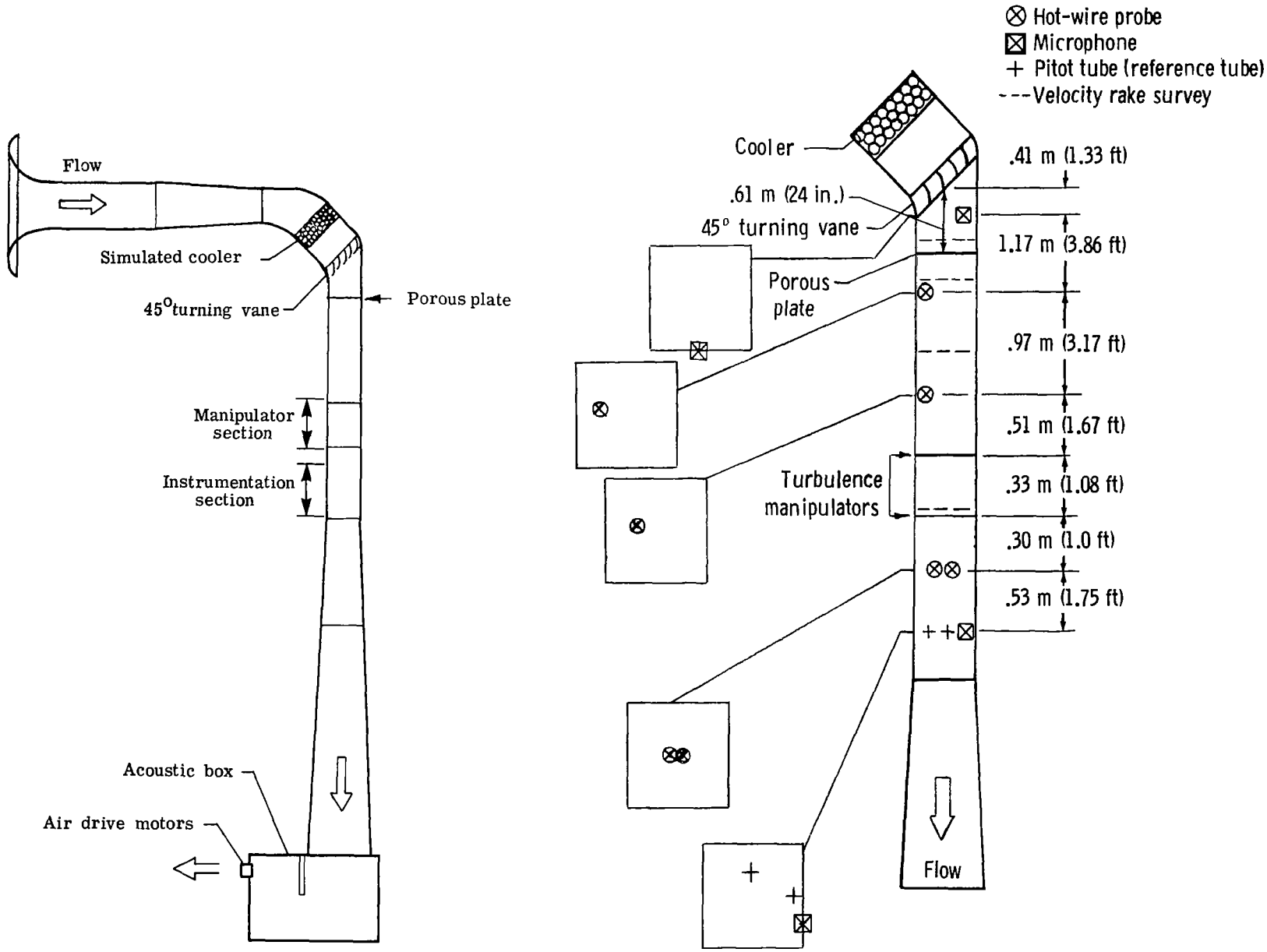

(a) Plan view of flow duct.

(b) General dimensions.

Figure 1.- One-half scale model used in turbulence reduction program.

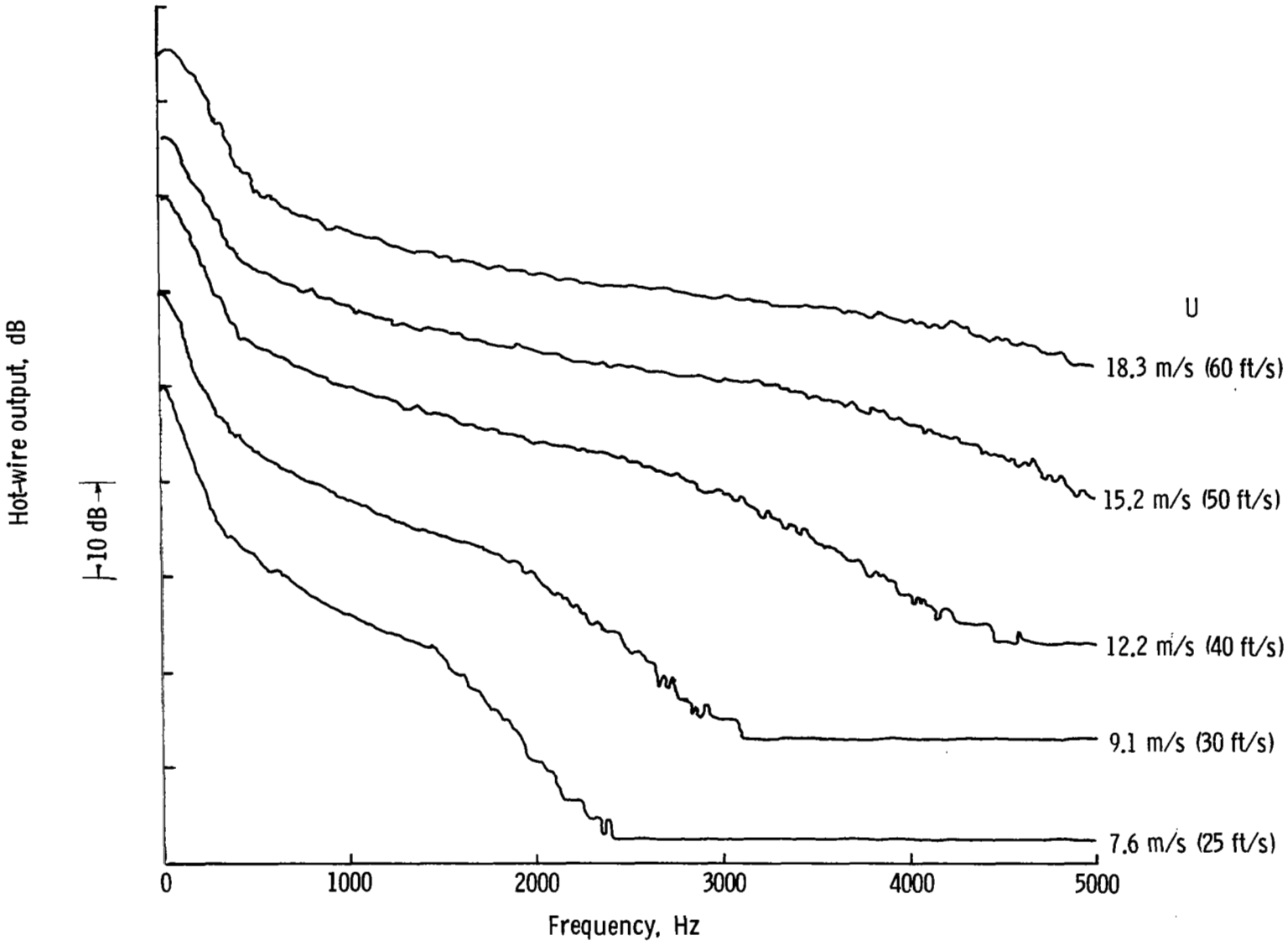

(a) Hot wire upstream of manipulator.

Figure 2.- Typical hot-wire and acoustic microphone spectra in flow stream for various speeds. Hot-wire spectra are for axial turbulence. Note 10-dB shift in ordinate origin for each speed range.

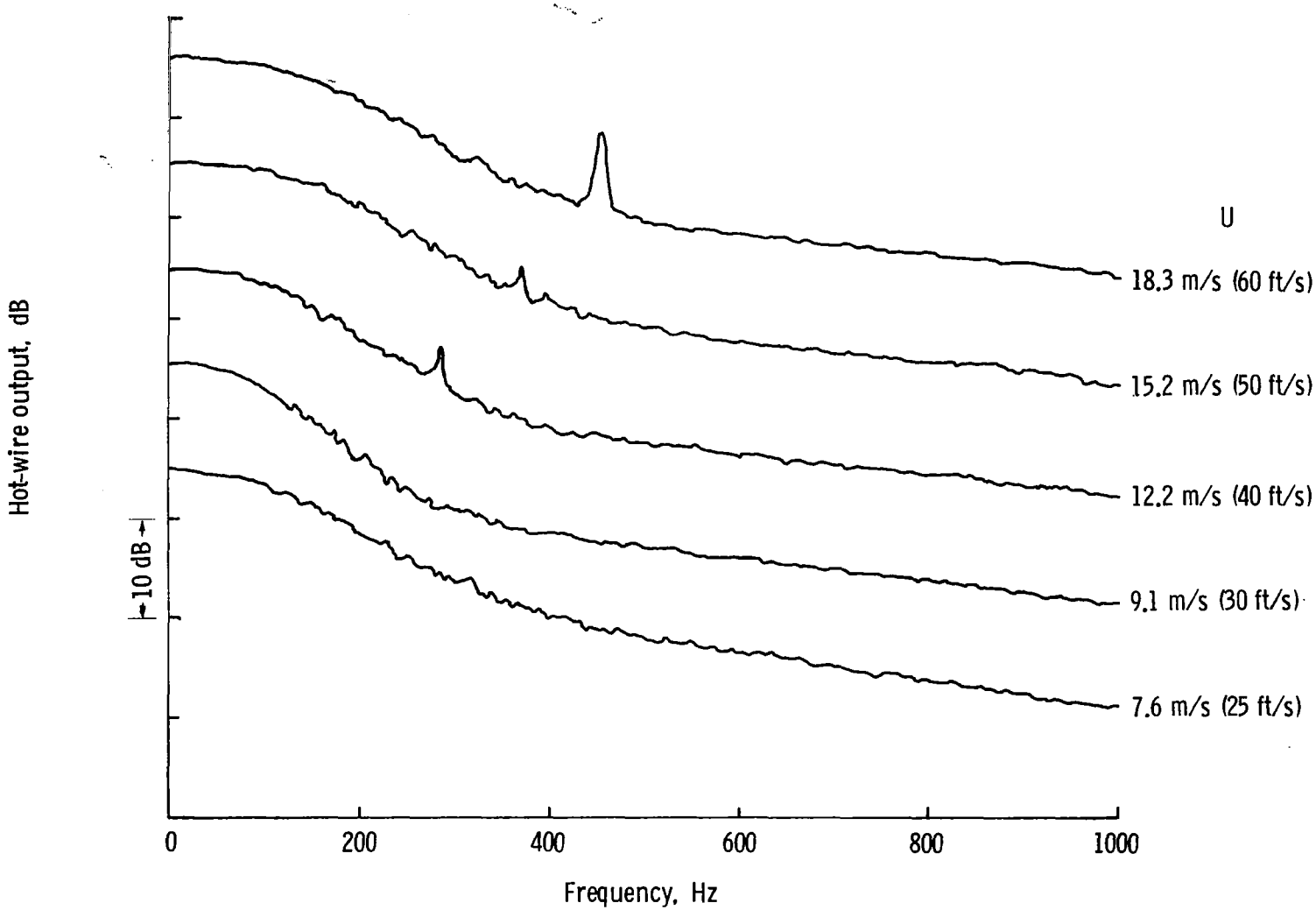

(b) Hot wire downstream of manipulator.

Figure 2.- Continued.

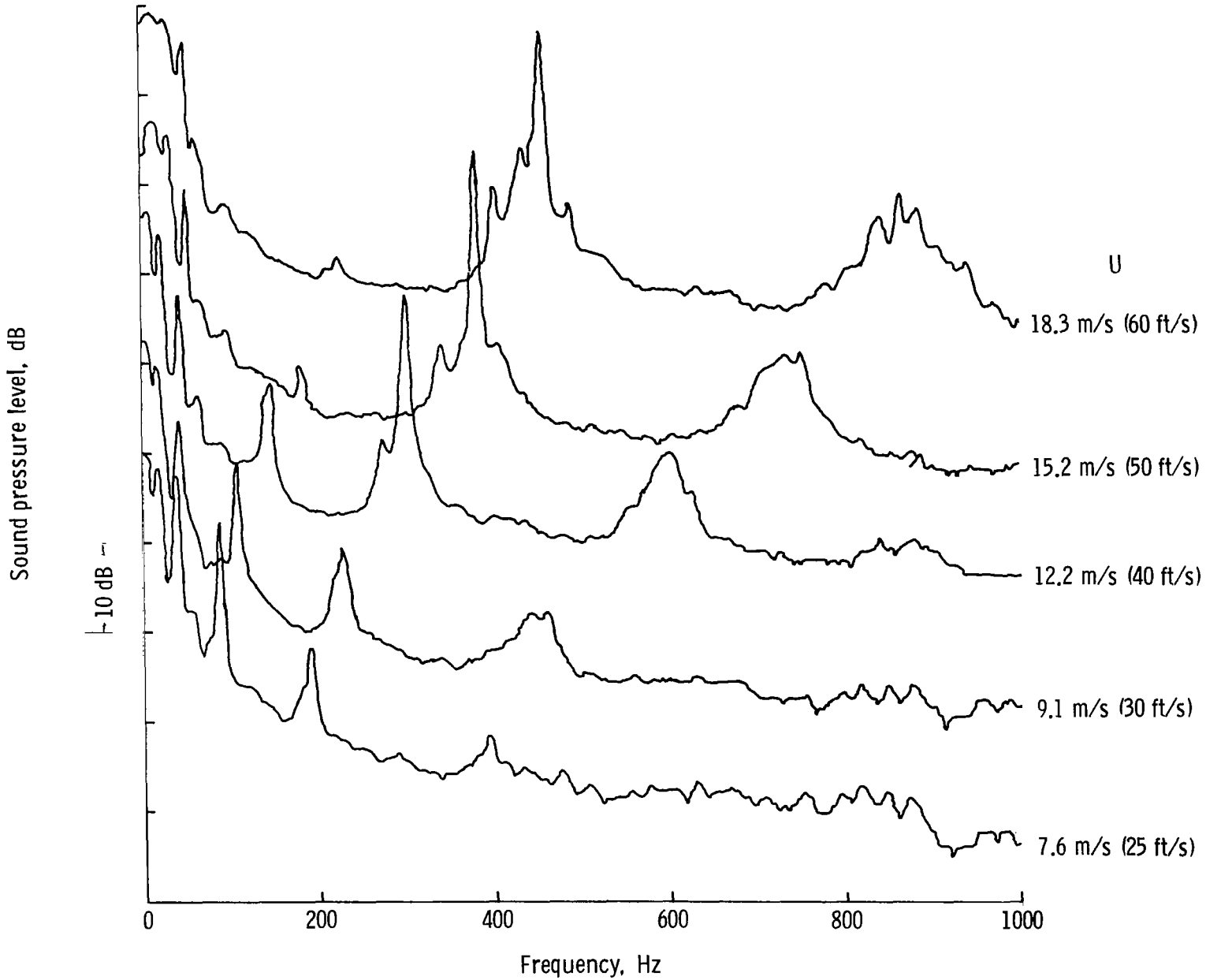

(c) Microphone downstream of manipulator.

Figure 2.- Concluded.

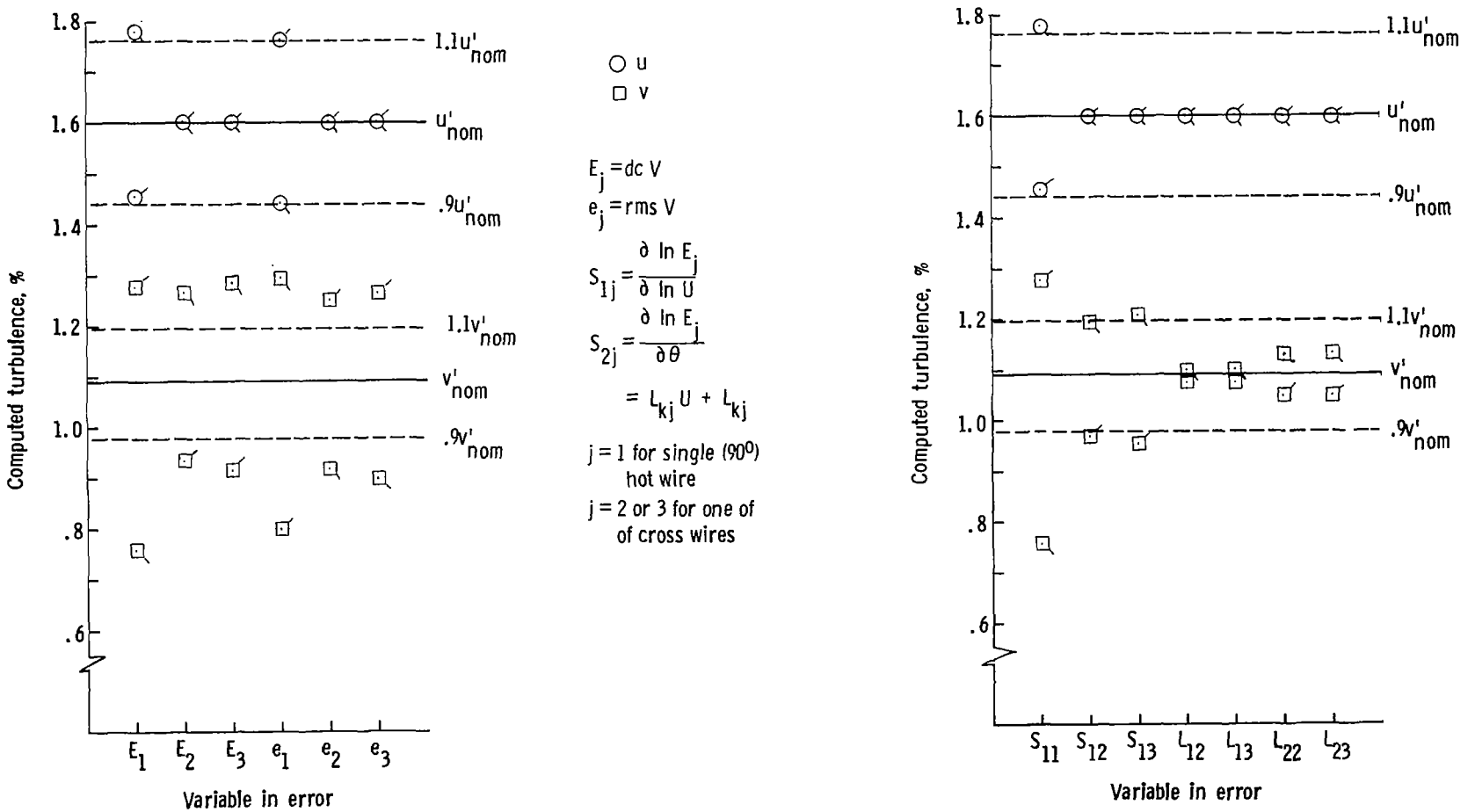

(a) Measured voltage variables.

(b) Calibration variables.

Figure 3.- Calculated turbulence using typical input values and introducing ±10-percent error for one variable (indicated on abscissa). Up flag on symbol corresponds to +10-percent error in one input variable and down flag corresponds to -10-percent error.

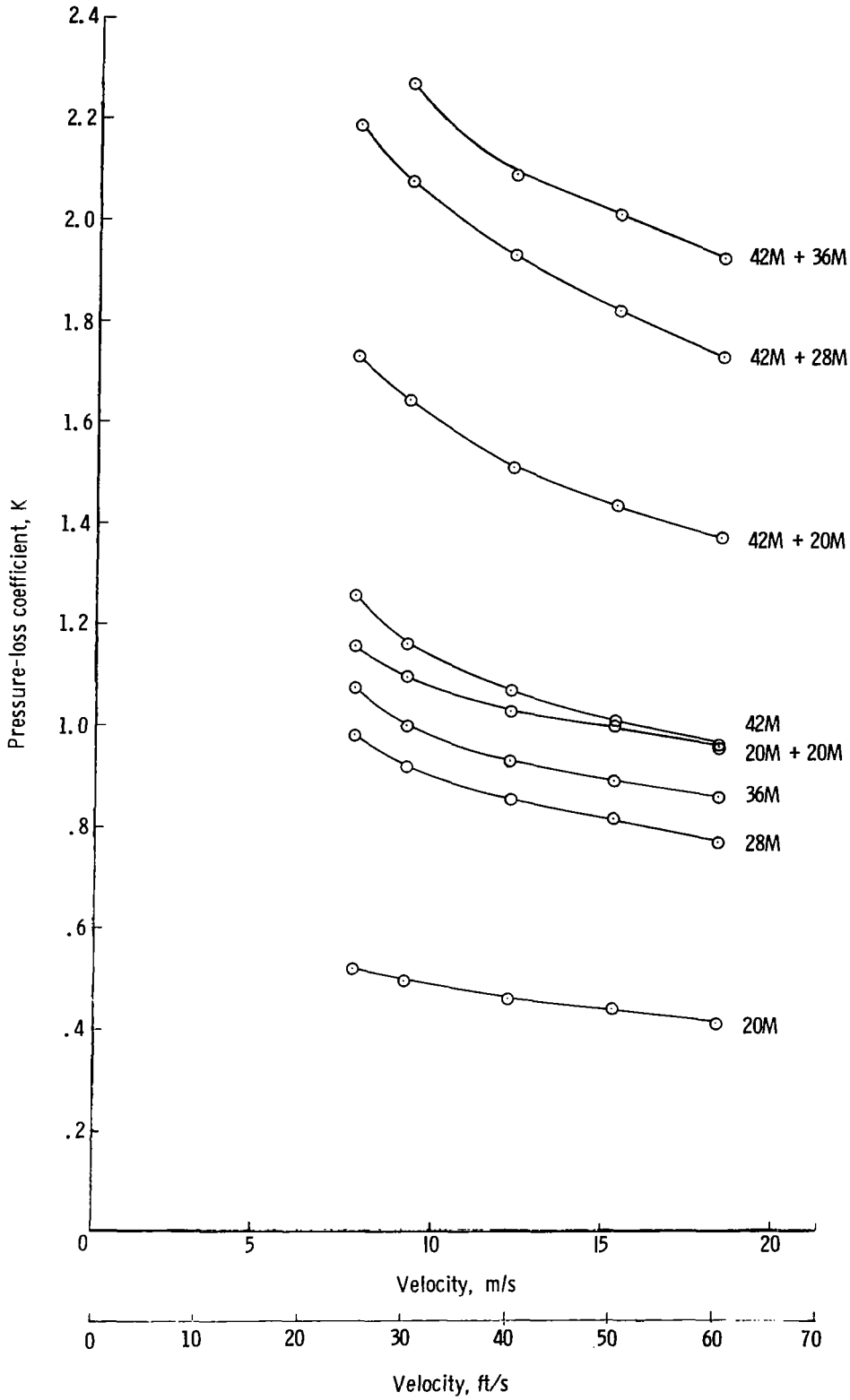

Figure 4.- Pressure-loss coefficient as function of duct velocity for various screens and screen combinations.

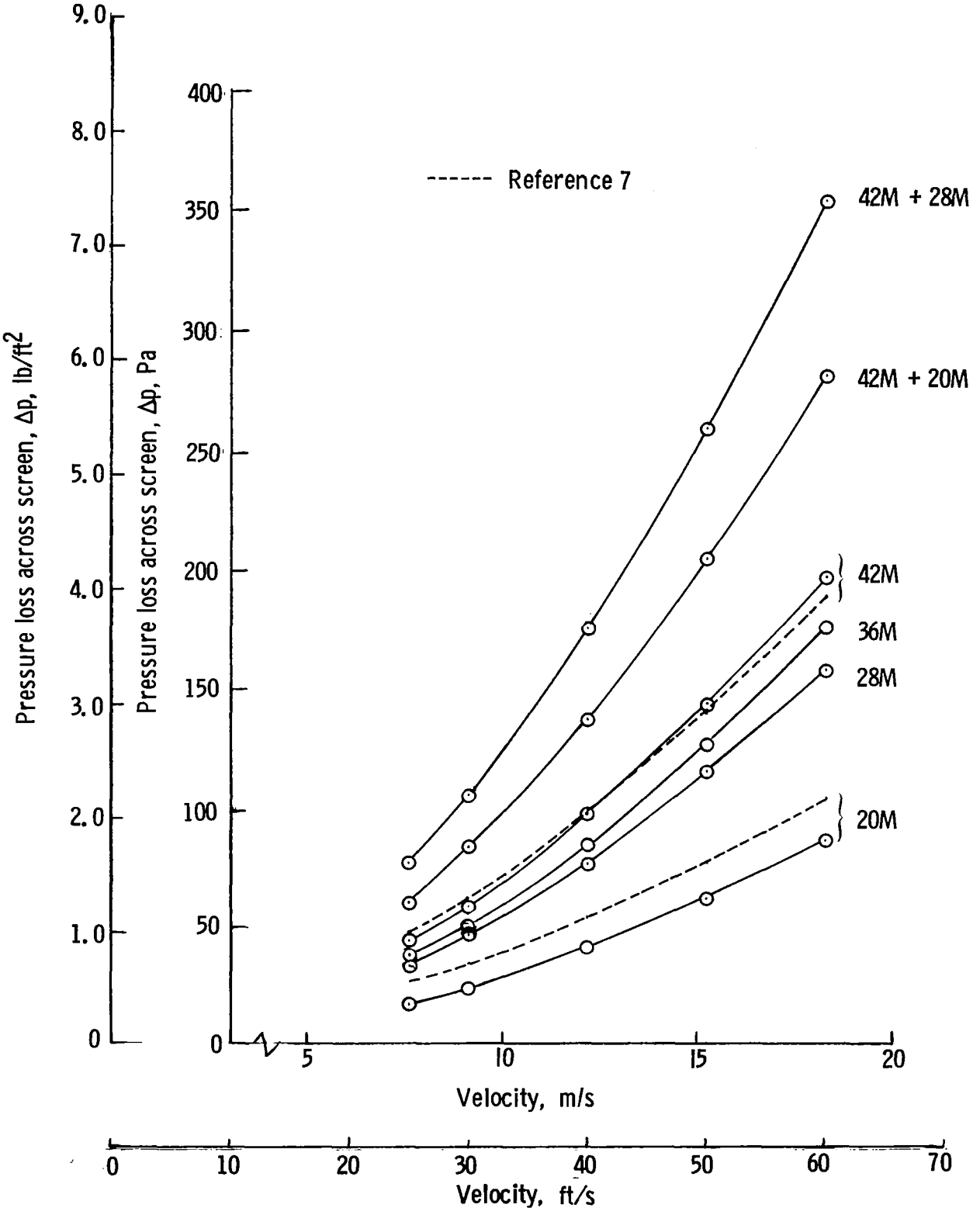

Figure 5.- Pressure loss across various screen and screen combinations as a function of duct velocity. Screen mesh indicated in figure.

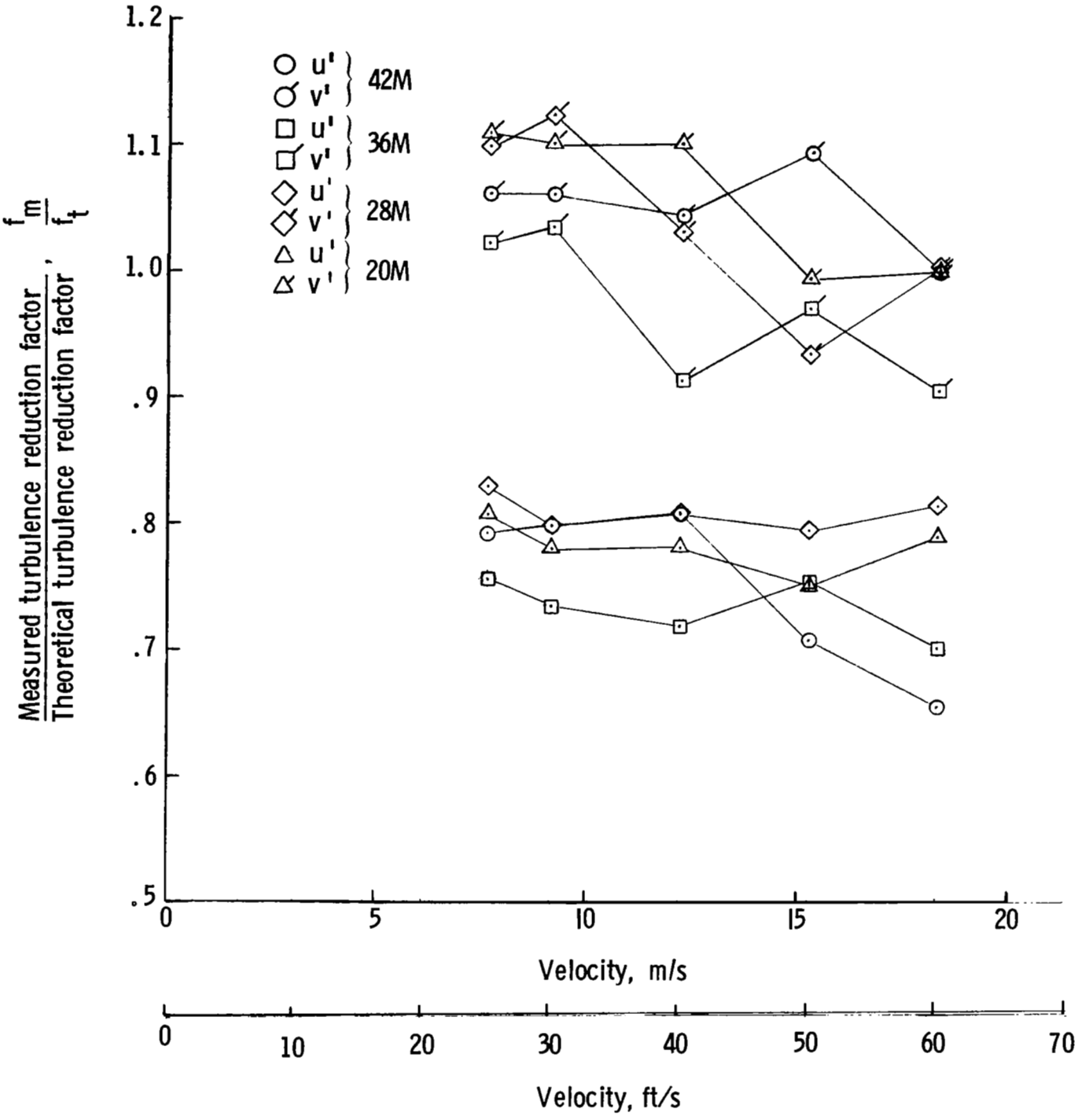

Figure 6.- Comparison of measured and theoretical turbulence reduction factors as function of velocity for various screen mesh sizes.

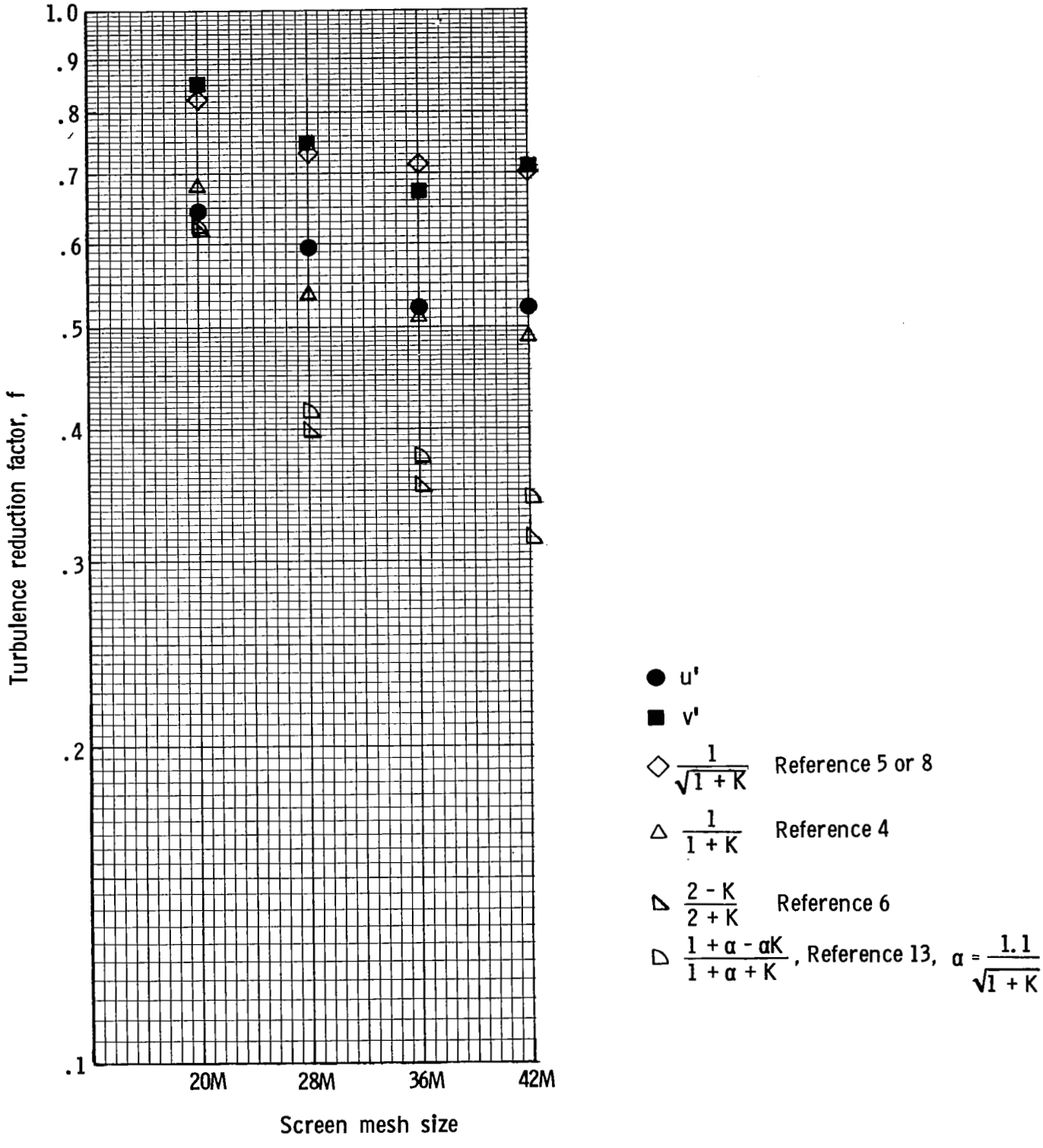

Figure 7.- Turbulence reduction factor for various screens.

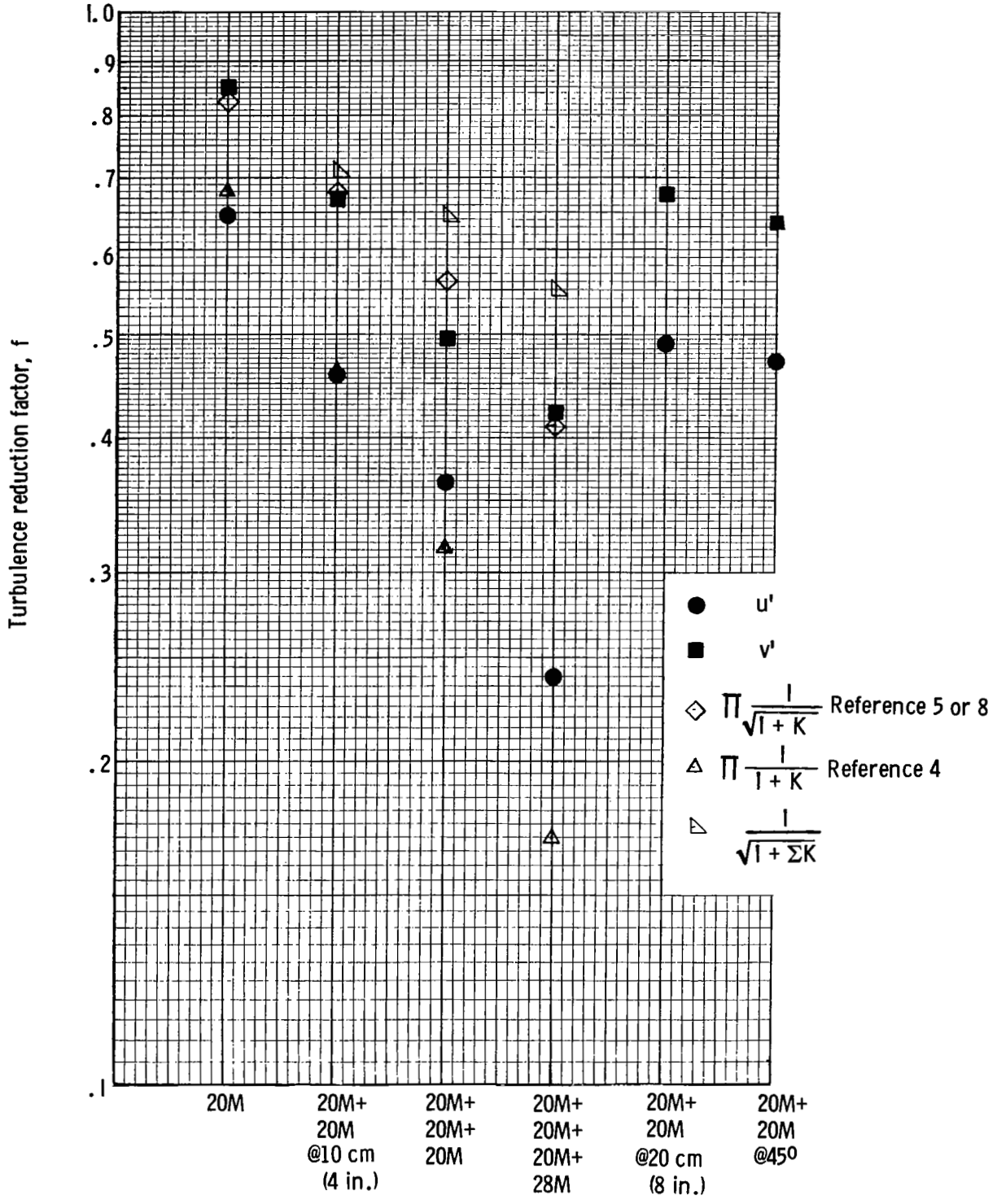

Figure 8.- Turbulence reduction factor for various screen and screen combinations. Note two 20M screens at different screen spacing and two 20M screens with the wire weaves at 45° to each other.

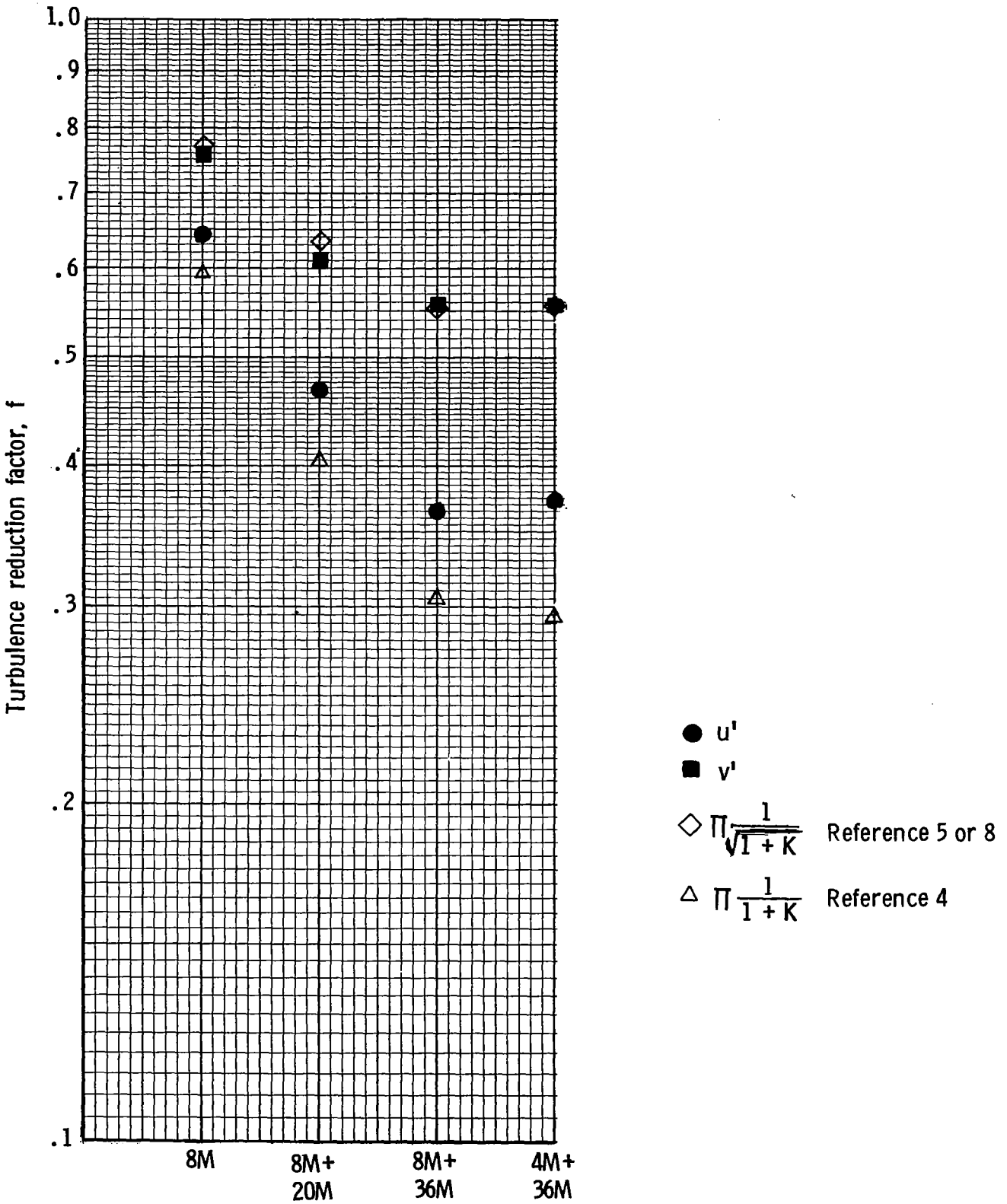

Figure 9.- Turbulence reduction factor for various screens and screen combinations with coarser mesh.

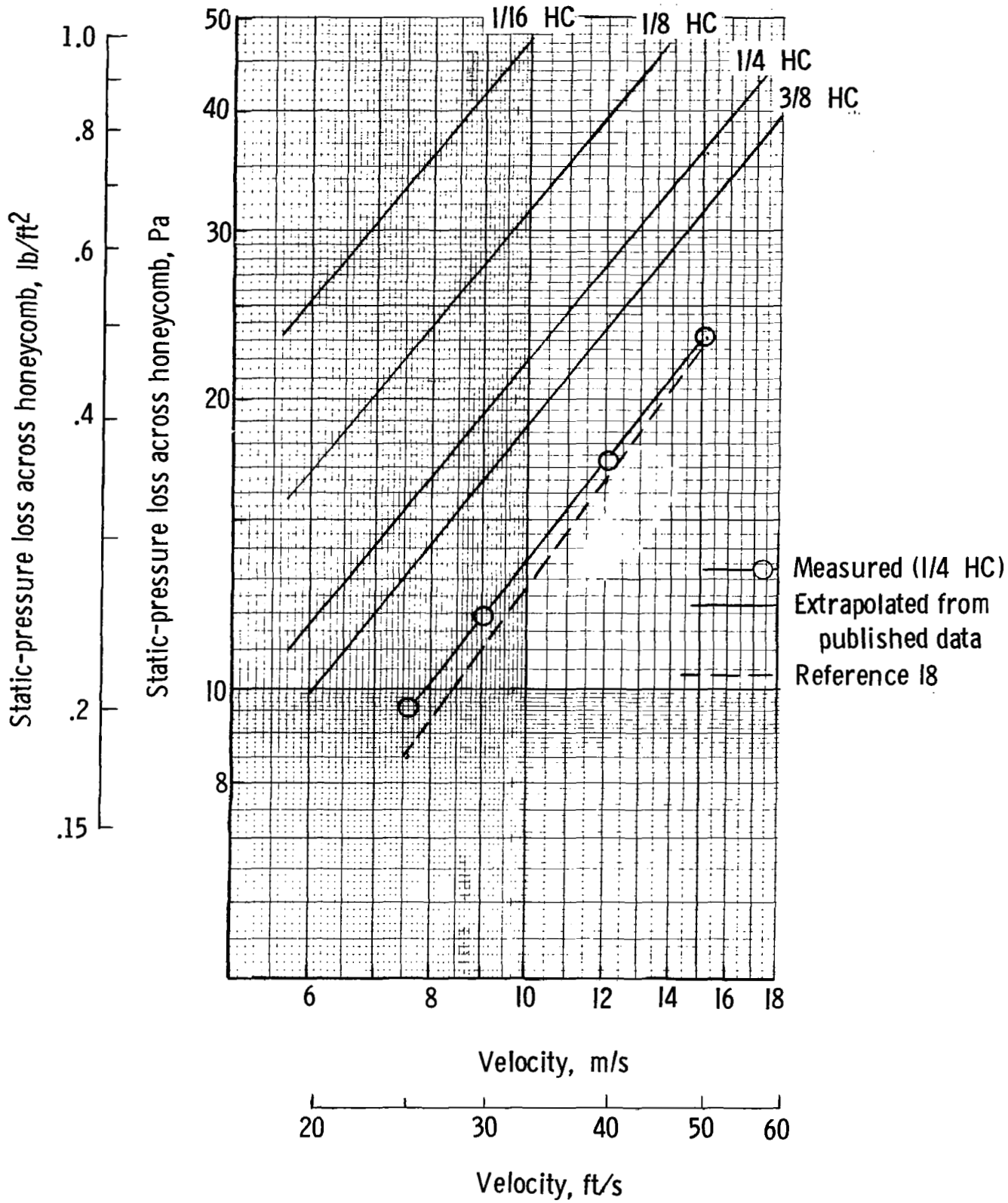

Figure 10.- Static-pressure loss across honeycomb as function of velocity.

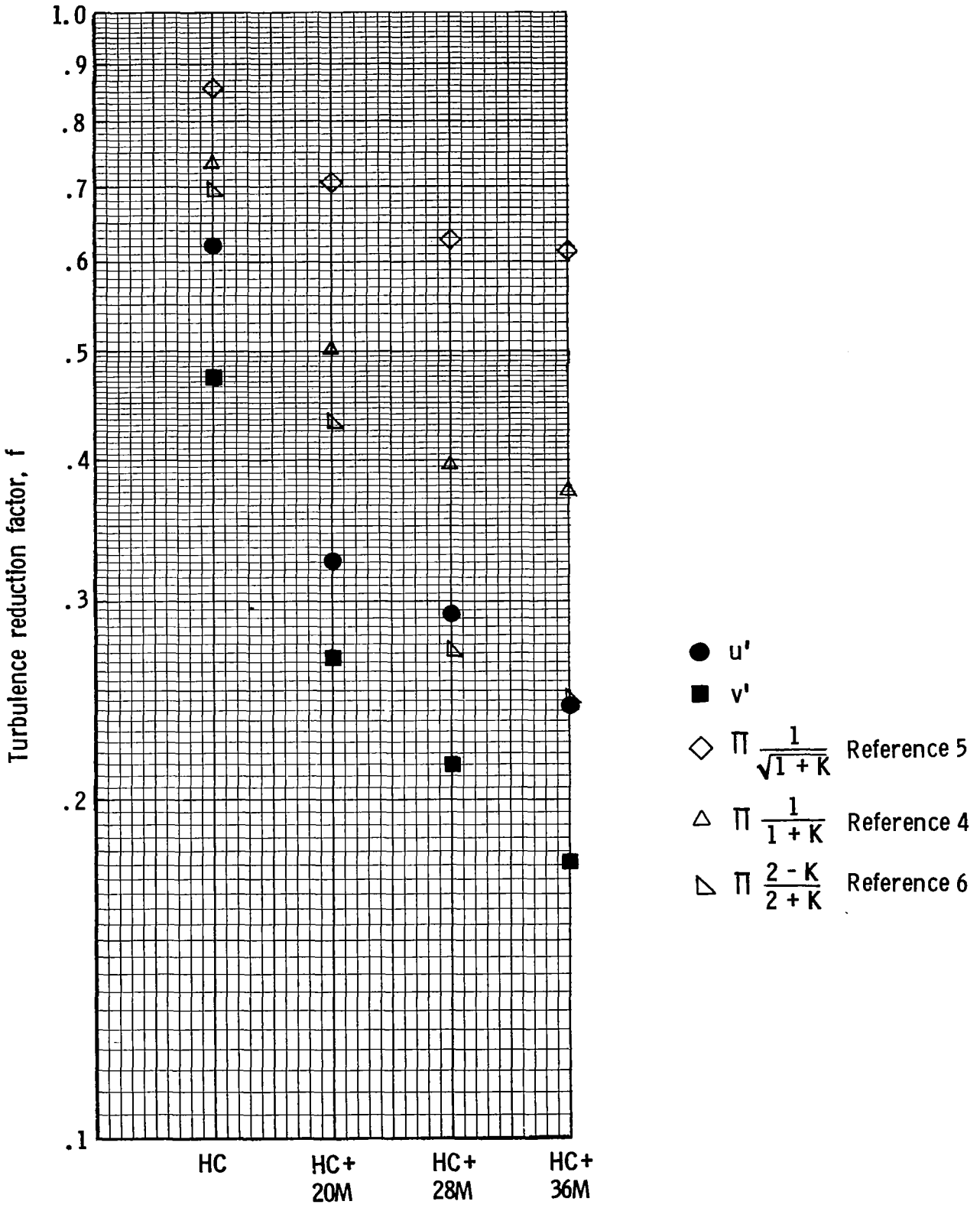

Figure 11.- Turbulence reduction factor for 1/4 HC alone and in combination with various screen mesh sizes.

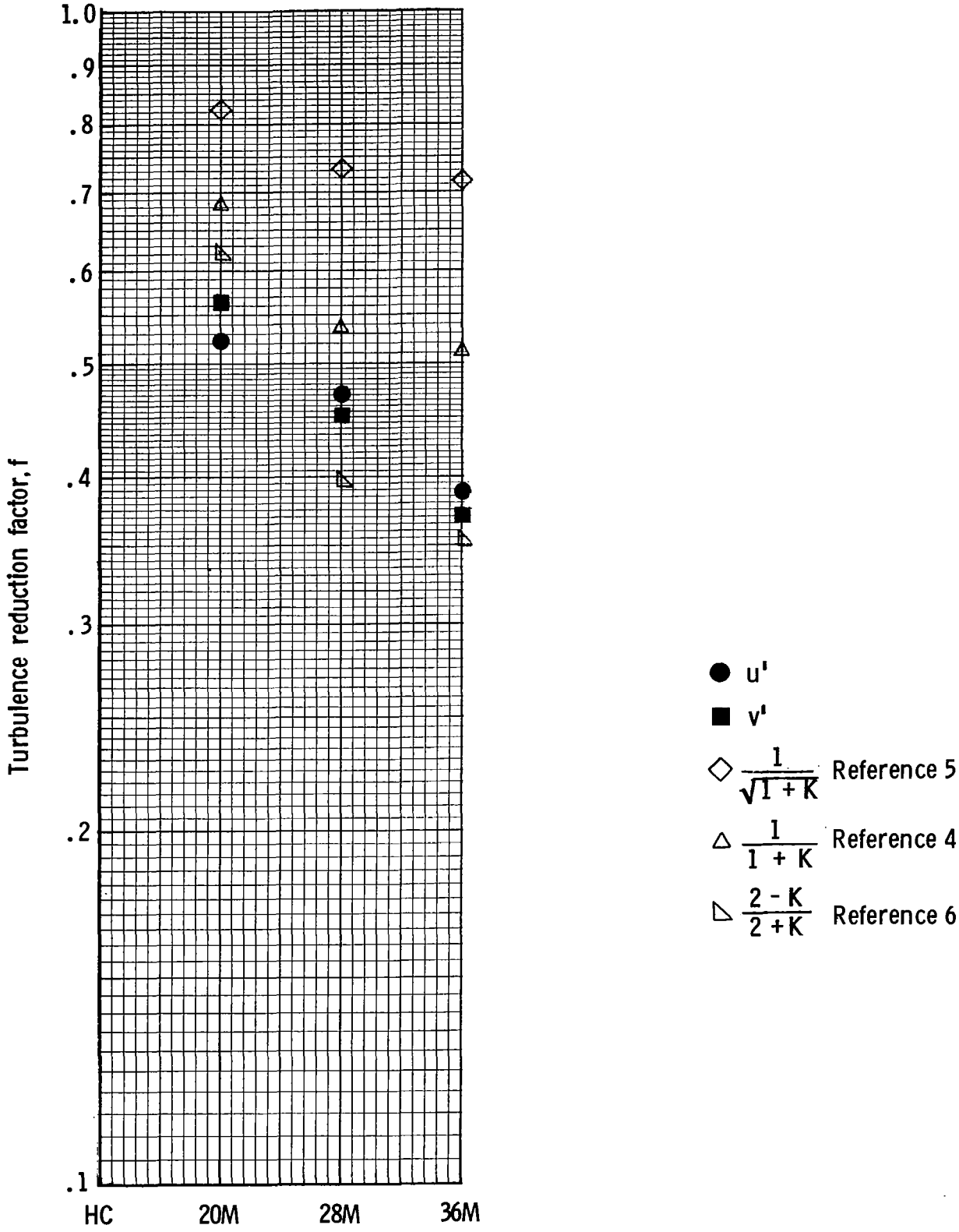

Figure 12.- Turbulence reduction factor for screens downstream of 1/4 HC. Turbulence reduction from HC is not included in screen turbulence reduction. (Turbulence downstream of HC is considered turbulence without manipulator.)

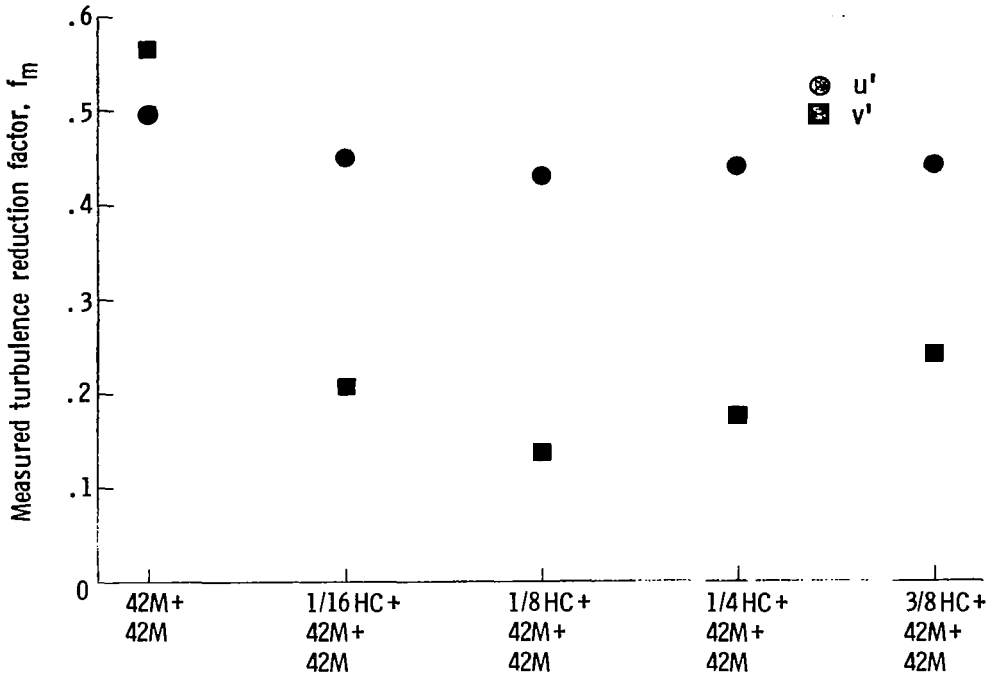

Figure 13.- Turbulence reduction factor for two 42M screens alone and in combination with various upstream honeycomb mesh sizes.

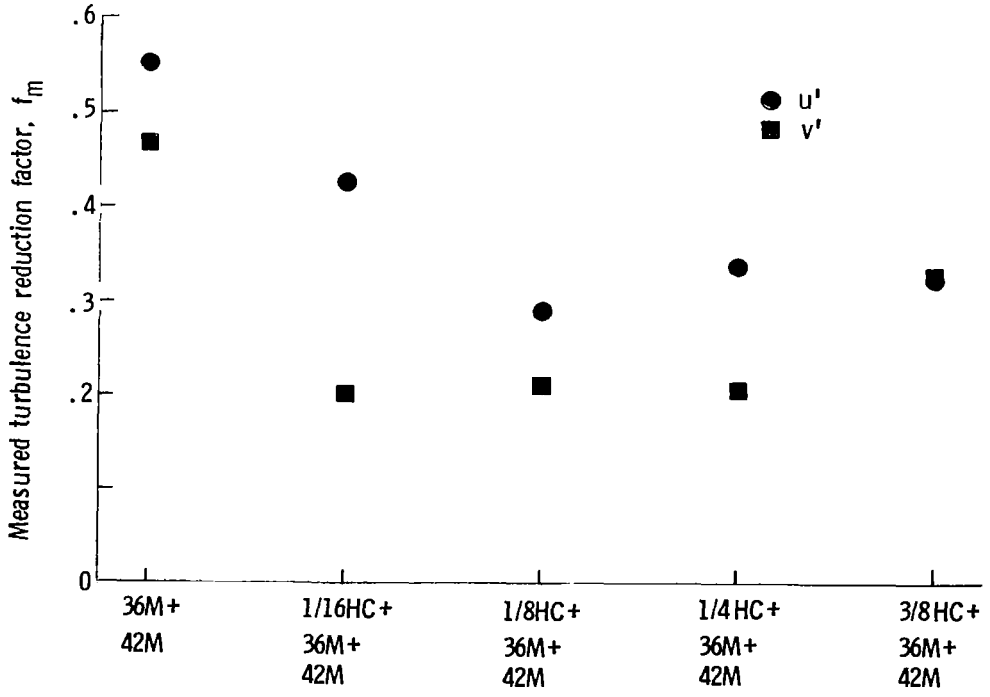

Figure 14.- Turbulence reduction factor for 36M and 42M screens alone and in combination with various upstream honeycomb mesh sizes.

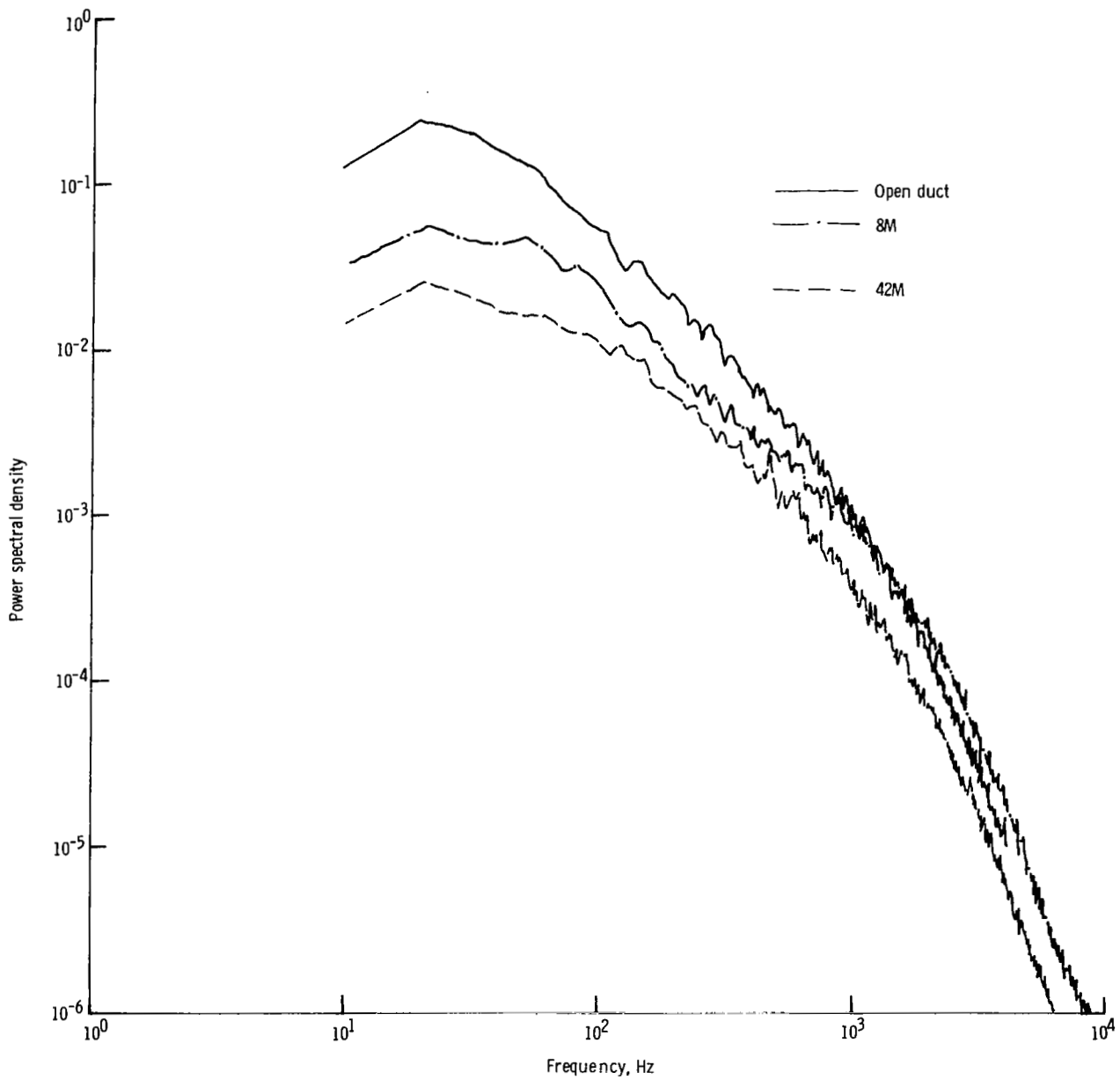

(a) Axial turbulence, u'.

Figure 15.- Spectra of turbulence for two screens and no screens. Coordinate scale relative to other presented spectra only.

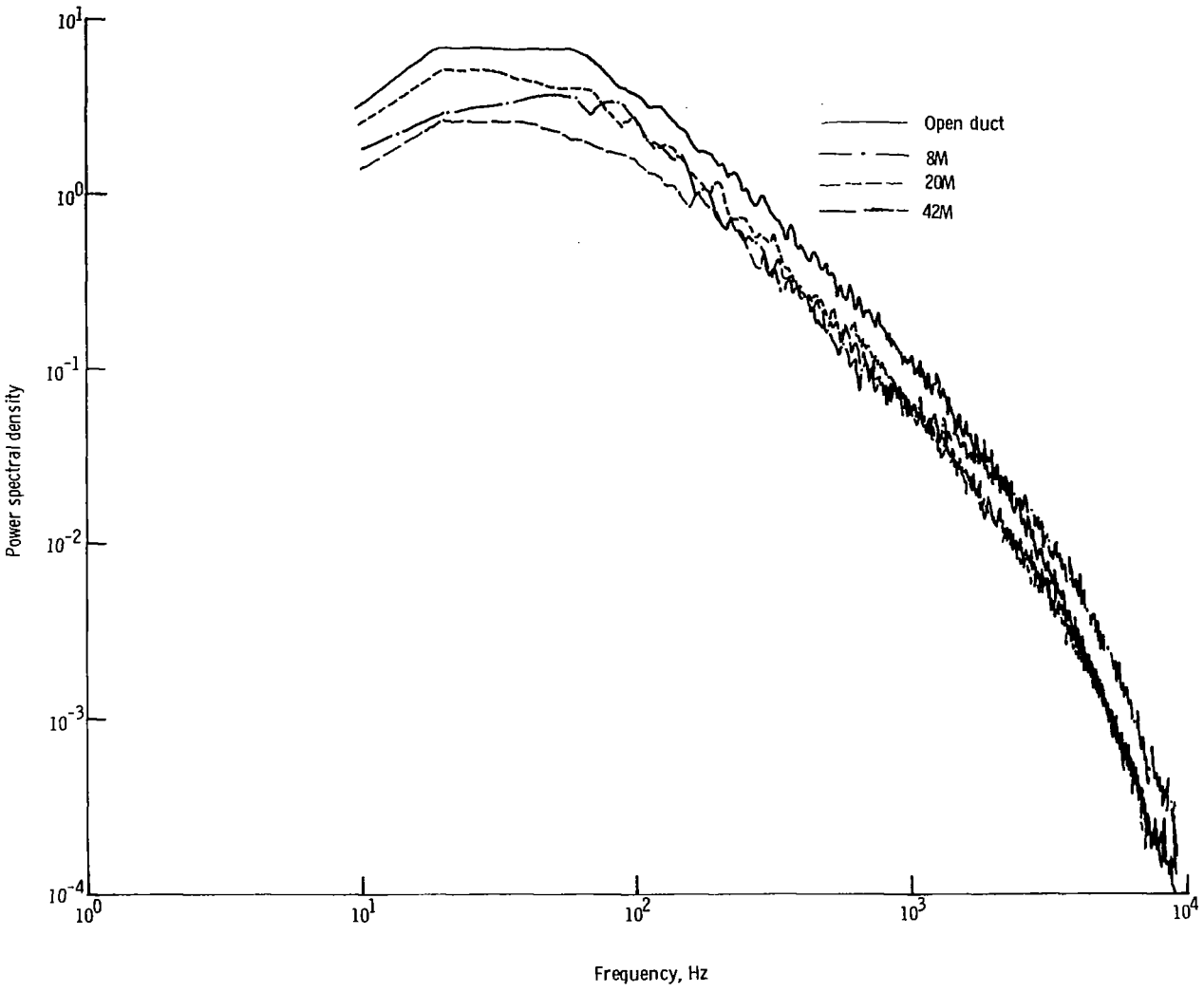

(b) Approximate lateral turbulence, v'.

Figure 15.- Concluded.

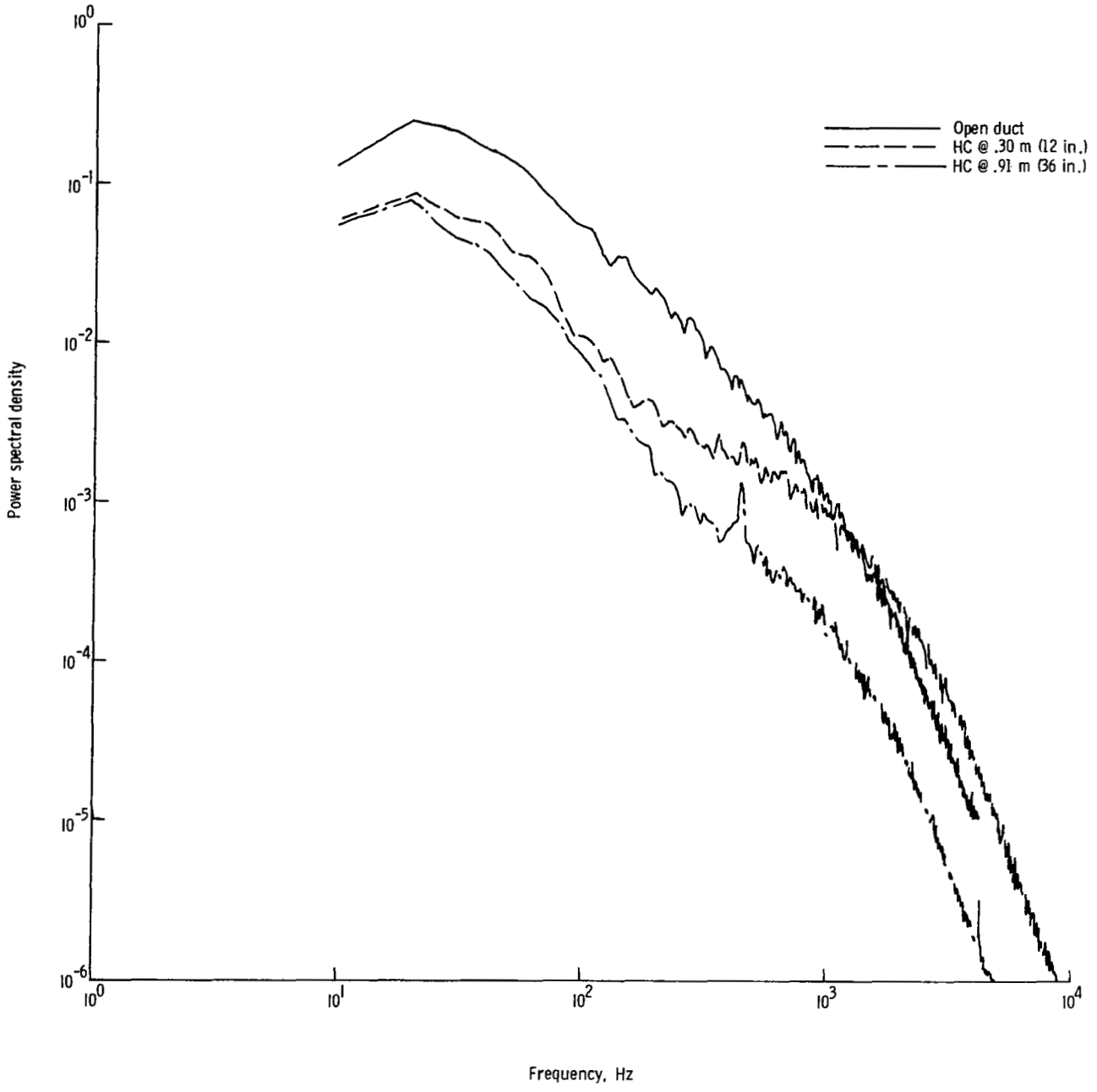

(a) Axial turbulence, u'.

Figure 16.- Spectra of turbulence for 1/4 HC at two downstream distances and no honeycomb. Ordinate scale relative to other presented spectra only.

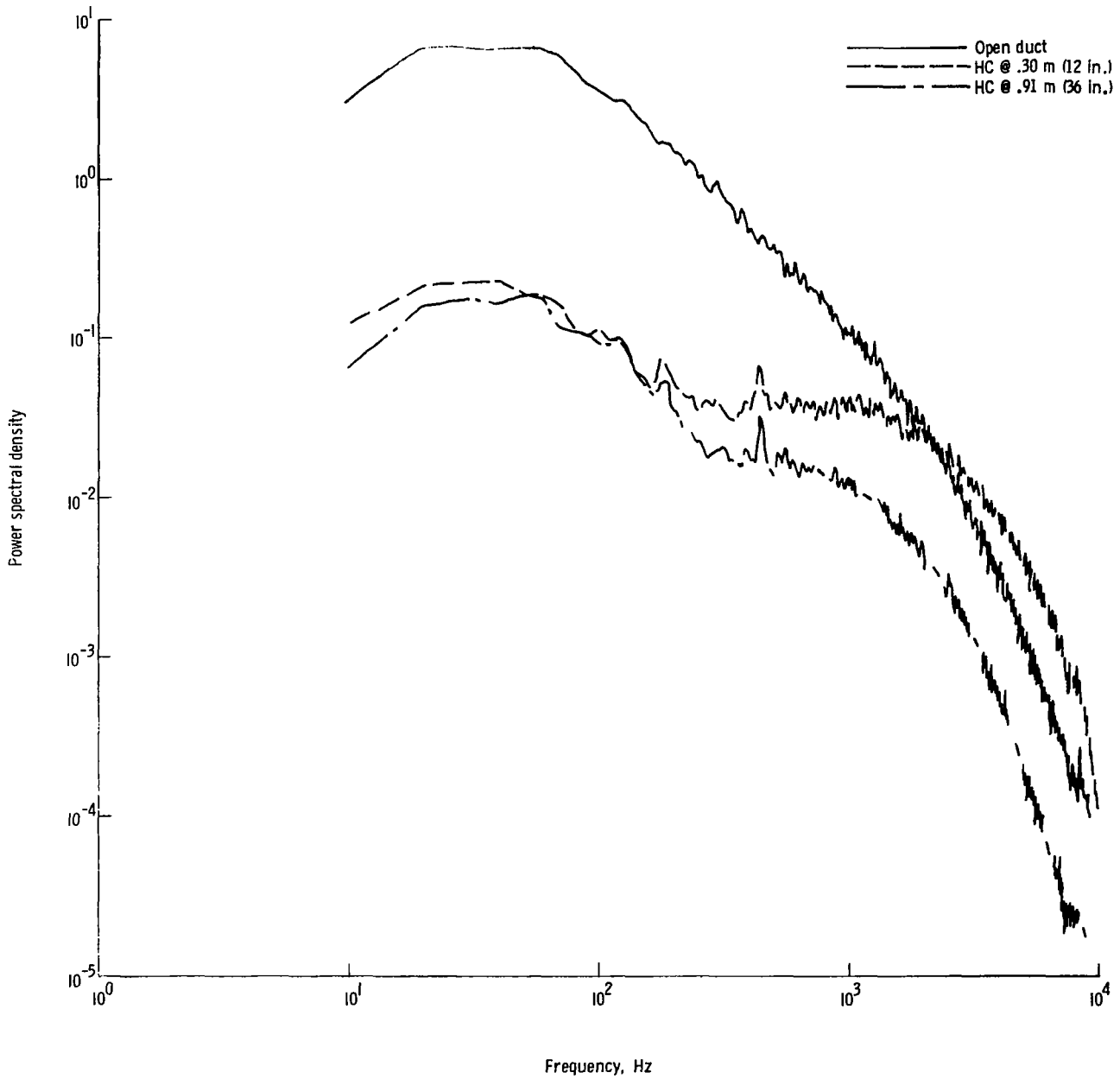

(b) Approximate lateral turbulence, v'.

Figure 16.- Concluded.

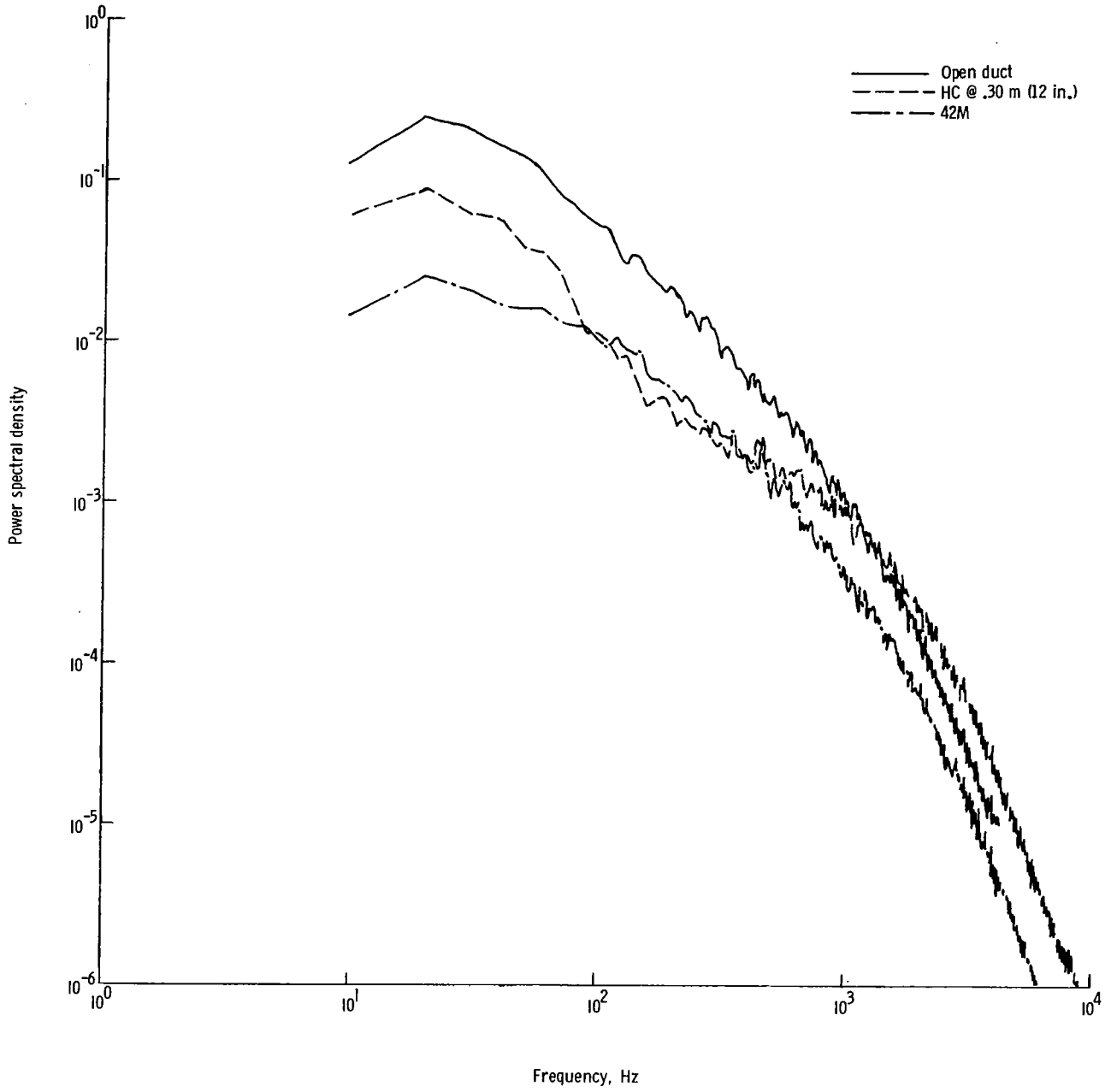

(a) Axial turbulence, u'.

Figure 17.- Comparison of spectra for open duct, honeycomb only, and screen only. Ordinate scale relative to other presented spectra only.

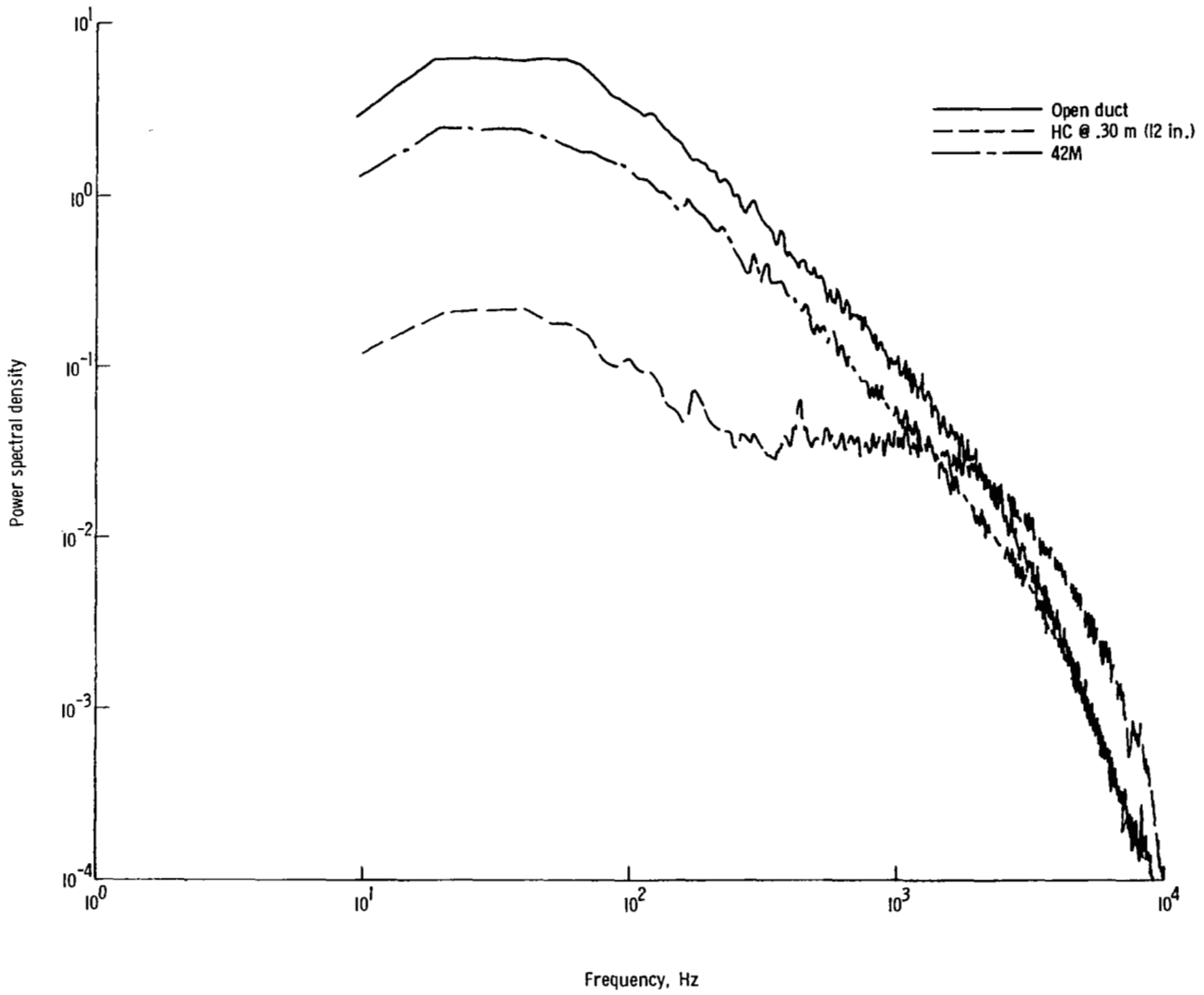

(b) Approximate lateral turbulence, v'.

Figure 17.- Concluded.

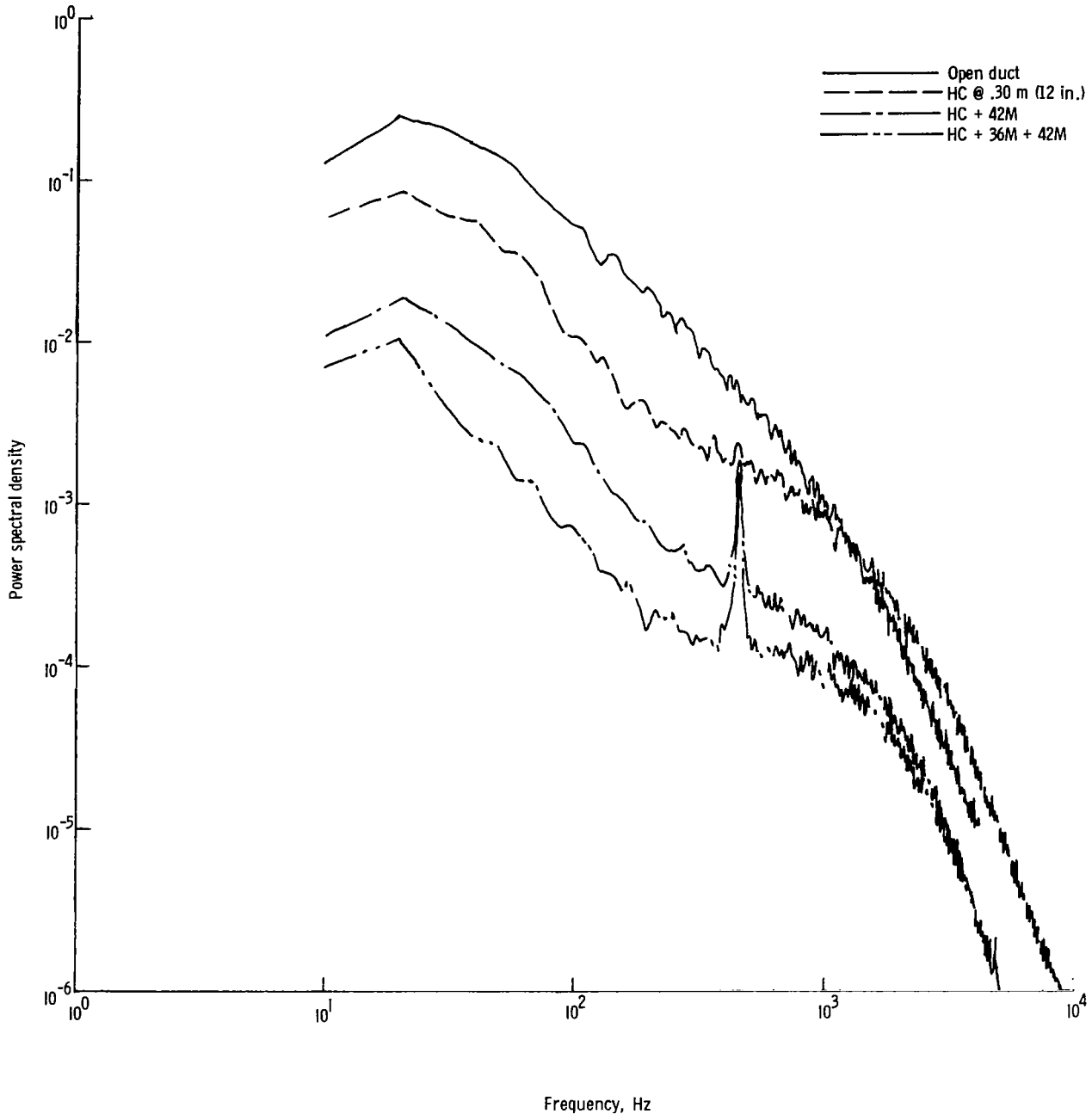

(a) Axial turbulence, u'.

Figure 18.- Comparison of spectra of turbulence for open duct, honeycomb only, and honeycomb with screens. Ordinate scale relative to other presented spectra only.

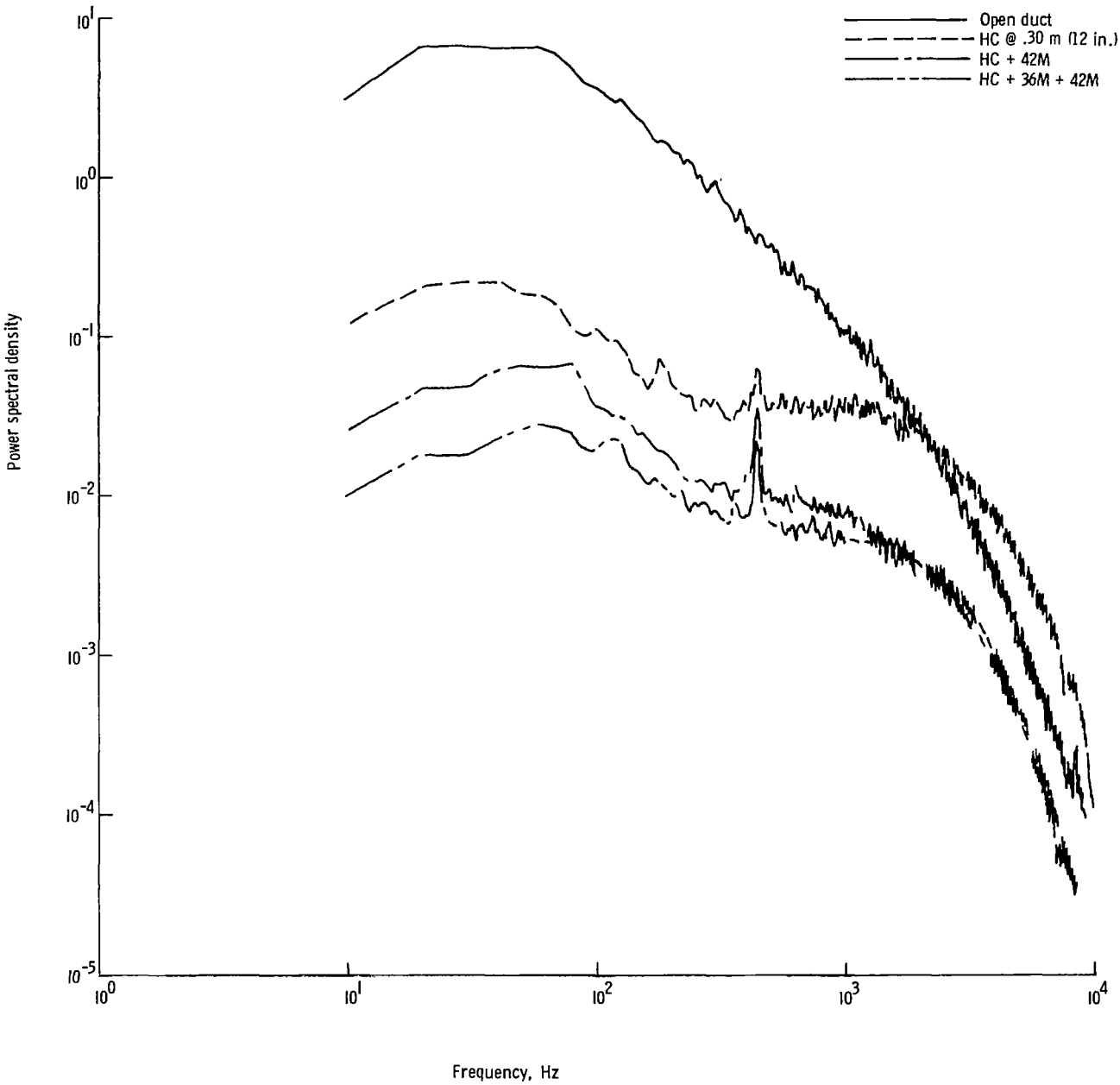

(b) Approximate lateral turbulence, v.

Figure 18.- Concluded.

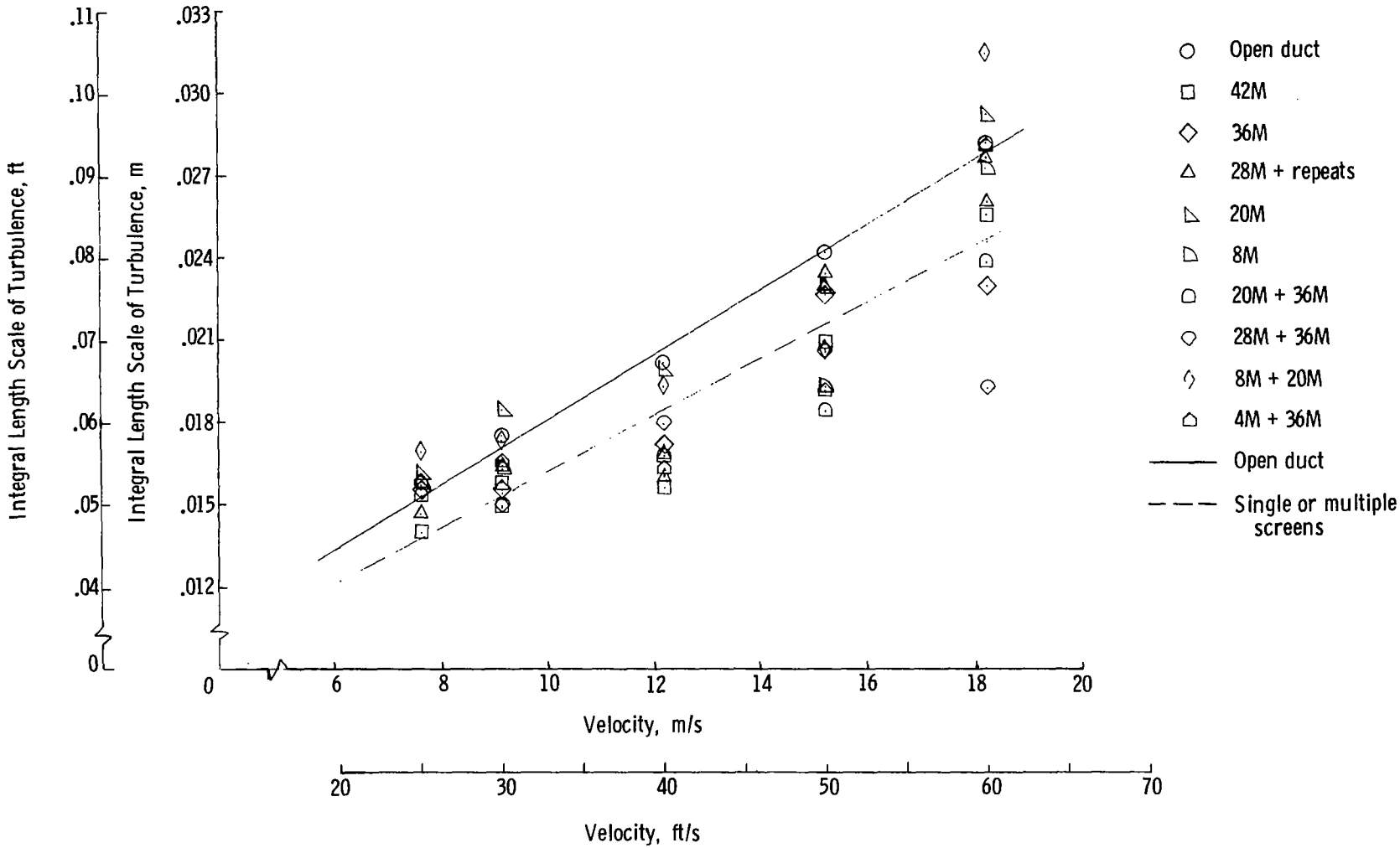

Figure 19.- Integral scale of turbulence versus duct speed for open duct and various screens. Least-square-fit straight-line through data shown.

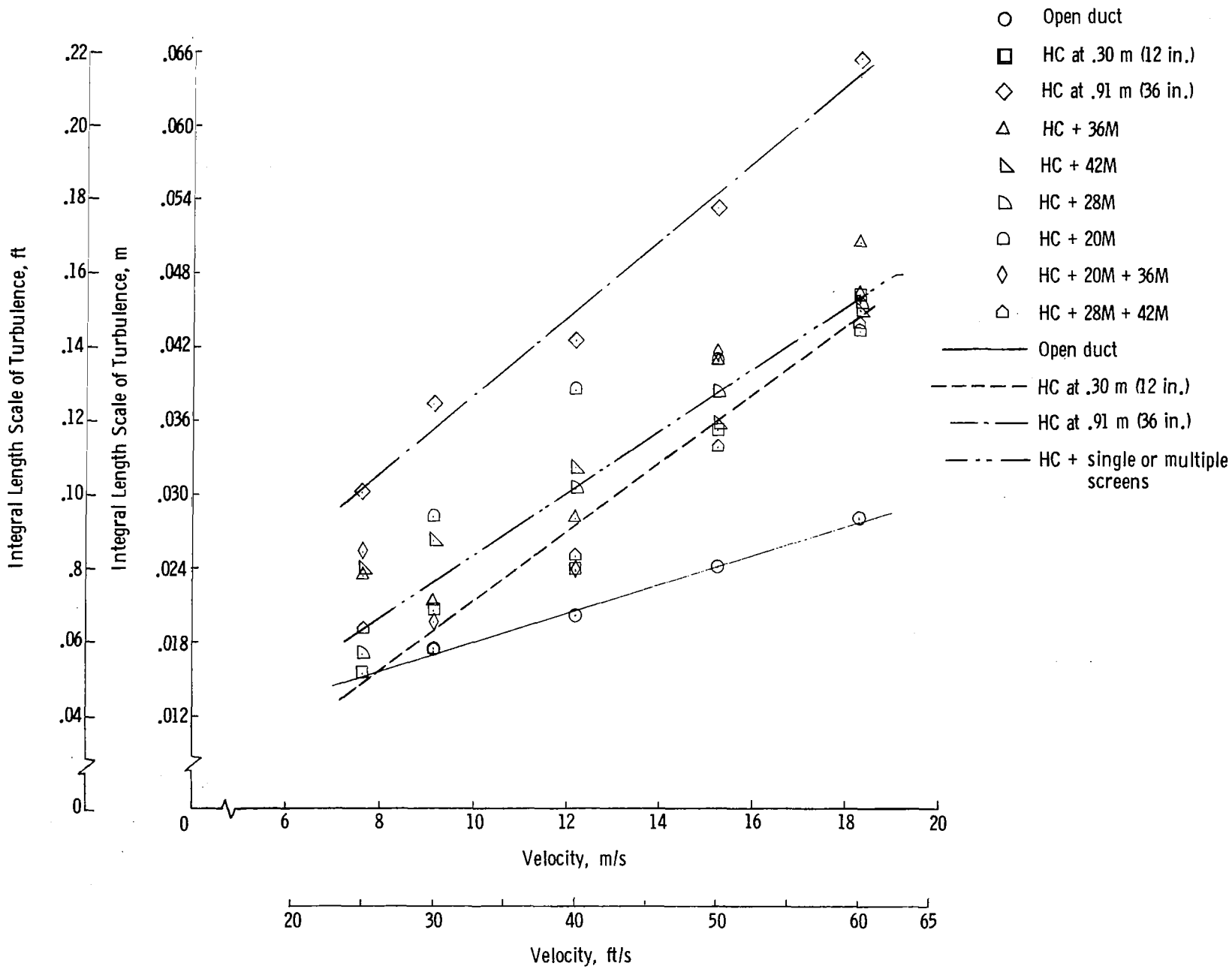

Figure 20.- Comparison of integral scale of turbulence for an open duct, honeycomb alone at two downstream distances, and for honeycomb-screen combinations. Least-square-fit straight-line through the data shown.

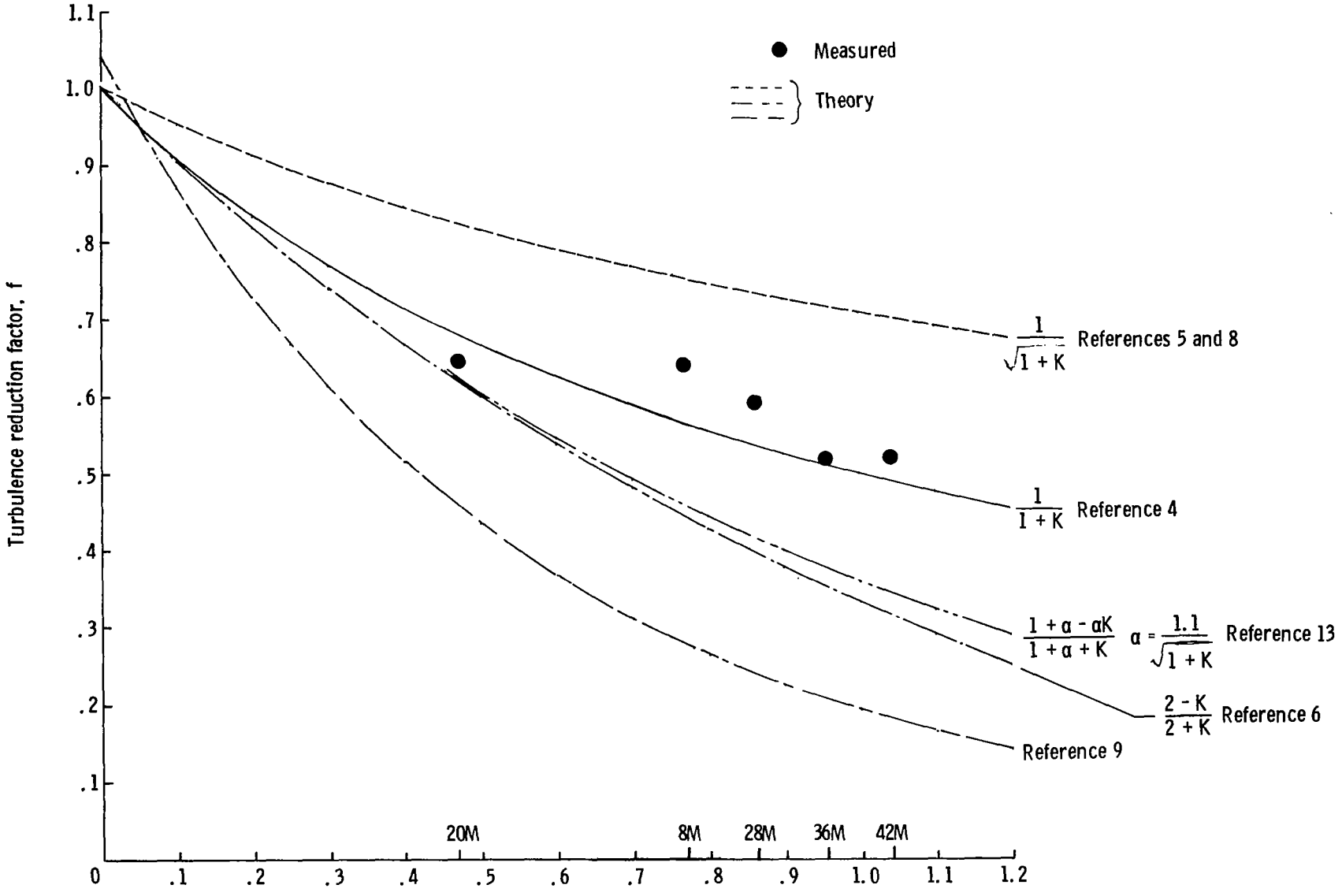

(a) Axial turbulence.

Figure 21.- Measured turbulence reduction compared with different theories.

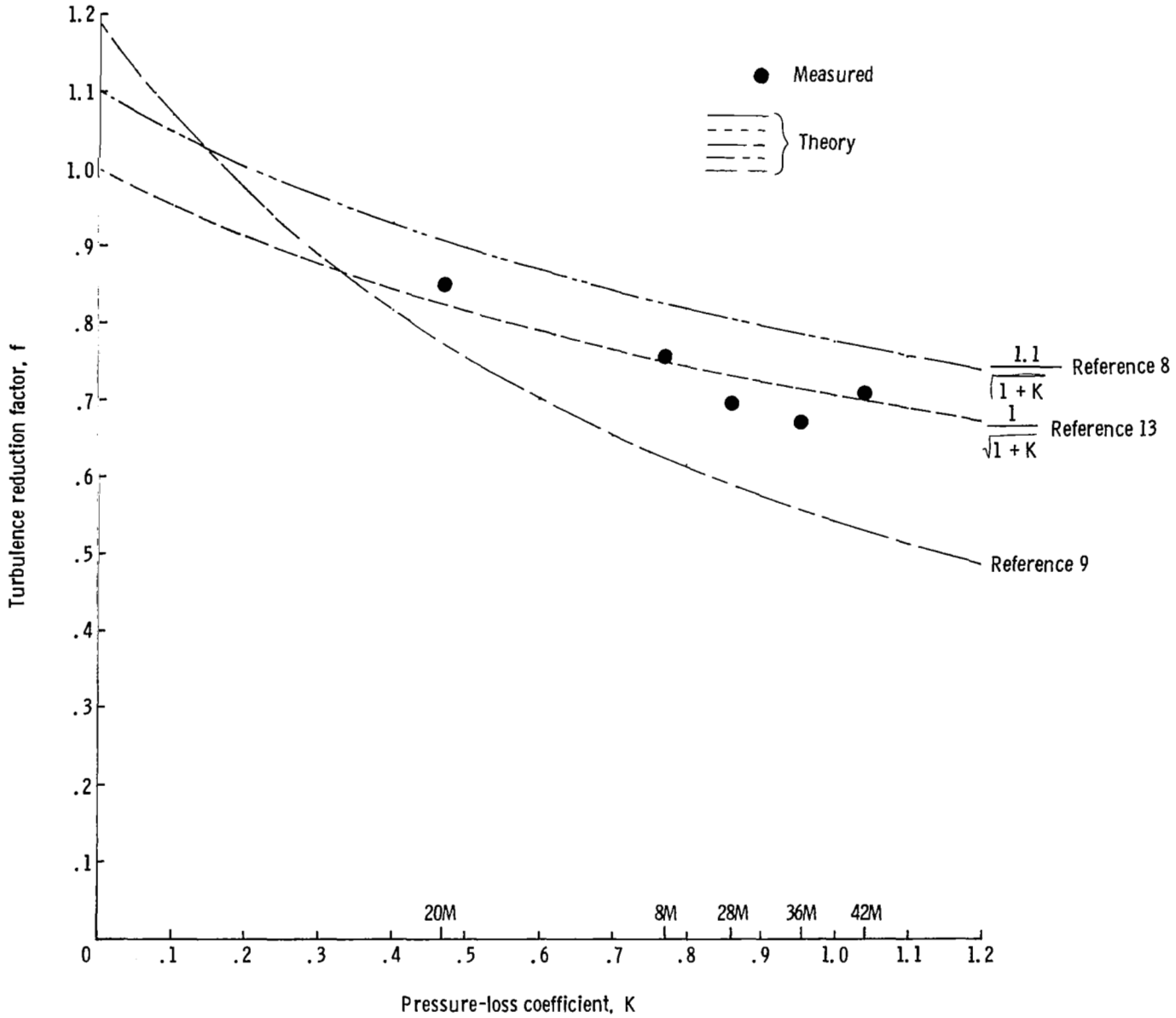

(b) Lateral turbulence.

Figure 21.- Concluded.

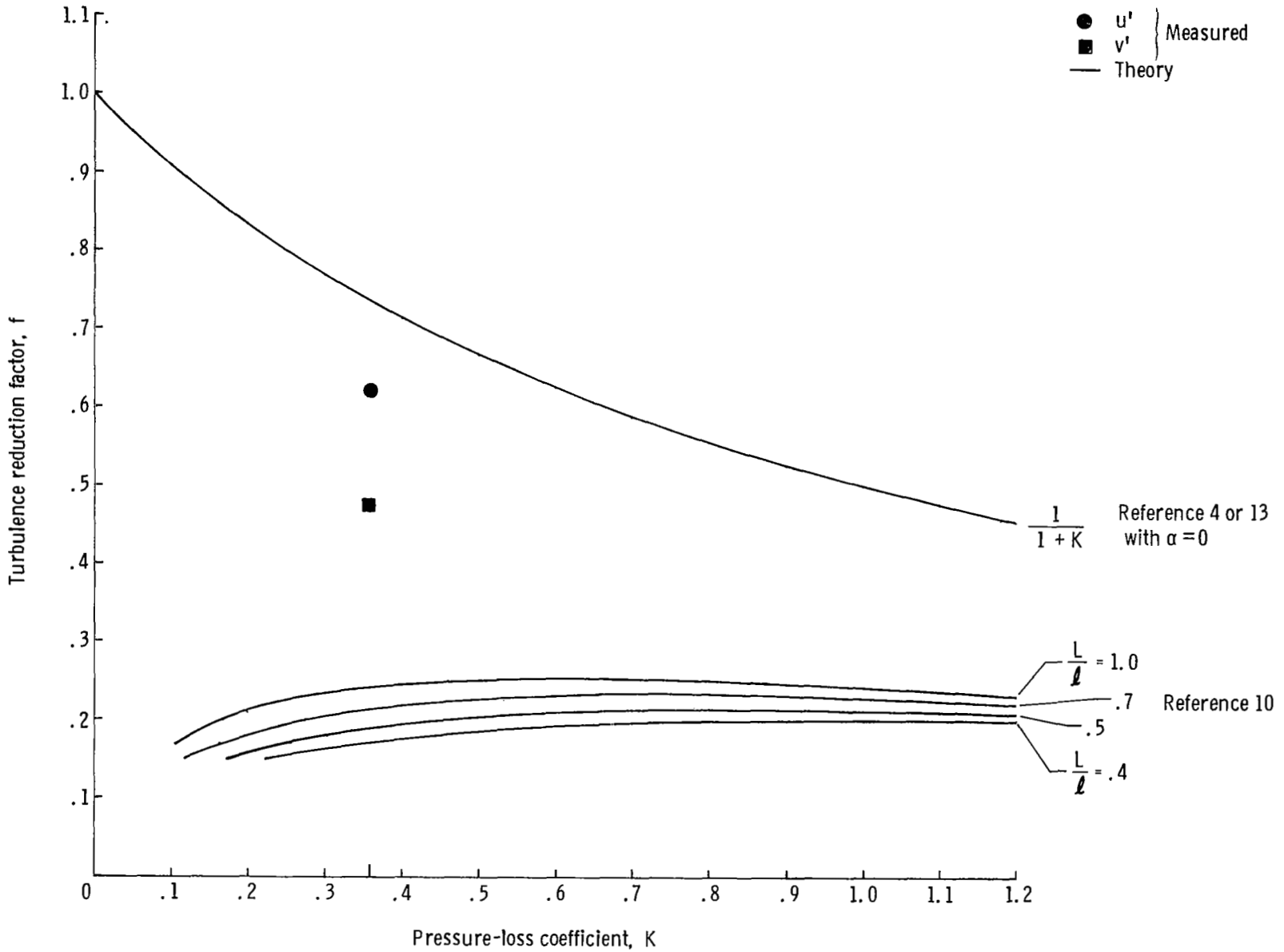

Figure 22.- Correlation of measured axial and lateral turbulence reduction with theory. 1/4 HC with cell depth of 3.8 cm (1.5 in.).